EXPERIMENTAL DETERMINATION OF THE PERTURBATION OF A PLASMA BY A PROBE

Roger G. Little
B.A., Colgate University
(1962)

SUBMITTED IN PARTIAL FULFILLMENT
OF THE REQUIREMENTS FOR THE DEGREE OF
MASTER OF SCIENCE
at the
MASSACHUSETTS INSTITUTE OF TECHNOLOGY
August, 1964

Signature of Author . . . . . .
Department of Geology and Geophysics, August 24, 1964

Certified by . . . . . .
Thesis Supervisor

Accepted by . . . . . .
Chairman, Departmental Committee on Graduate Students

ABSTRACT

EXPERIMENTAL DETERMINATION OF THE PERTURBATION OF A PLASMA BY A PROBE

by

Roger G. Little

Submitted to the Department of Geology and Geophysics on August 21, 1964, in partial fulfillment of the requirements for the degree of Master of Science.

An attempt is made to experimentally establish the validity of J. Waymouth's theory of the perturbation of a plasma by a probe. The perturbation caused by a large-probe which violates Langmuir's condition that probe size be smaller than the mean free paths of all plasma particles is examined with a small-probe that satisfies Langmuir's conditions. Electron density and plasma potential are determined as a function of distance from the large-probe and are found to correlate well with the predictions of Waymouth's theory. Also, applying Waymouth's correction to the data derived from a perturbing probe to get the true plasma parameters is found to be valid.

Thesis Supervisor: Francis Bitter

Title: Professor of Geophysics

Table of Contents

Title page	1
Abstract	2
Table of Contents	3
Acknowledgements	5
Glossary	6
I. Introduction	7
II. Langmuir Probe Theory	9
A. Assumptions	9
B. Positive Probe	9
C. Negative Probe	10
Fig. 1 Langmuir Probe Characteristic	11
D. Spherical Probe	12
E. Discharge Parameters	12
III. Waymouth's Theory	14
A. Perturbation of Electron Density	15
B. Perturbation of Plasma Potential	17
IV. The Experiment	19
A. The Discharge Tube	19
Fig. 2 Photo of Discharge Tube	20
Fig. 3 Diagram of Discharge Tube	21
Fig. 4 Small-probe	22
Fig. 5 Large-probe	22
B. Waymouth's Conditions Satisfied	23
C. Probe Measurement Technique	24
Fig. 6 Circuit Diagram	25
Fig. 7 Probe Curve	27
D. Sequence of Measurements	26
E. Method of Determining Parameters	28
F. Waymouth-Bitter Theory	28
V. Experimental Results Compared to Theory	29
A. The Method	29
B. Calculated Curve Fit	30
Fig. 8 Q_e, Q_i and Q_T vs. T_i	31

Fig. 9 Large Probe Curve Best Fit: Cathode-side 32
Fig.10 Large Probe Curve Best Fit: Anode-side 33
C. Small-probe Determination of Q Values 34
Fig.11-13 Small-probe Q_T's: Cathode-side 35

Fig.14-16 Small-probe Q_T's: Cathode-side 36

Fig.17-19 Small-probe Q_T's: Anode-side 37

Fig.20-22 Small-probe Q_T's: Anode-side 38

D. The Comparison 39
Fig. 23 Comparison : Cathode-side 40
Fig. 24 Comparison : Anode-side 41
Fig. 25 Q_e vs. V_s/V_e 42

E. The Potential Perturbation 43

Fig. 26 Calculated $\Delta V/V_e$ vs. V_p/V_e 44

Fig. 27 Plasma Potential vs. r/r_p : Cathode-side 45

Fig. 28 Plasma Potential vs. r/r_p : Anode-side 46

Fig. 29 Composite: Large-probe at Floating Potential 47

Fig. 30 Composite: Large-probe near Plasma Potential 48

F. Plasma Density from Large-probe Data 49
Table I. Large-probe Electron Saturation Current Correction: C-S 51
Table II. Large-probe Electron Saturation Current Correction: A-S 51

G. High Ion Temperature 53

VI. Inherent Complications 55
Fig. 31 Intensity Measurements: Cathode-side 56
Fig. 32 Intensity Measurements: Anode-side 57
Fig. 33 Electron Temperature Compared to Intensity: Cathode-side 59
Fig. 34 Electron Temperature Compared to Intensity: Anode-side 59
Fig. 35 Plasma Potential Minus Floating Potential: Cathode-side 61
Fig. 36 Plasma Potential Minus Floating Potential: Anode-side 62

VII. Conclusion 63

Appendix I Tube Processing 66
Appendix II Calculation of Sheath Thickness 67
Appendix III Constructed Large-probe Curve 68

References 69

Acknowledgements

This work could not have been done without the help of Dr. J. F. Waymouth and Professor Francis Bitter.

The discharge tube was constructed in the Research Laboratory of Electronics glass shop through the efforts of Laurence Ryan and Pat Doucette. George Leach handled the probe constructions.

The help of Laszlo Massey in the preparation of the diagrams is also appreciated.

The work was sponsored by the United States Government through contracts with the Research Laboratory of Electronics and the National Magnet Laboratory.

GLOSSARY

Symbol	Definition
n	Density of electrons or ions in neutral plasma
n_o	Density of electrons or ions in the unperturbed plasma
n_p	Density of electrons or ions at the sheath boundary (i.e., at the probe)
μ_e, μ_i	Electron, ion mobility
Γ_e, Γ_i	Particle current density of electrons or ions
V_e, V_i	Voltage equivalent of electron, ion temperatures in the plasma $\left(\frac{kT_e}{e}, \frac{kT_i}{e}\right)$
D_a	Ambipolar diffusion coefficient
r_p	Large-probe radius
V_s	Potential difference across the sheath, positive when probe is positive with respect to plasma outside the sheath
V_o	Potential of the unperturbed plasma
V_p	Potential of the plasma at the sheath boundary (i.e , at the probe)
ΔV	$V_p - V_o$ perturbation of the plasma potential by the probe

I Introduction

A primary diagnostic tool in gas discharge study is the electrostatic probe which can be biased positively or negatively with respect to a reference potential of the discharge, usually one of the electrodes. The resulting current-voltage curve or probe characteristic can be analyzed to give various important parameters of the discharge such as plasma density, potential, and temperature.

Probe technique was introduced by Mott-Smith and Langmuir[1] in 1924. The critical assumption upon which their development is based, is that the mean free paths of all plasma particles are large with respect to probe dimensions. When this assumption is valid, the probe is screened from the plasma by a space-charge sheath and does not effect the plasma beyond the sheath edge. Plasma parameters determined from the probe characteristic are those of the undisturbed plasma. When this condition is violated, density gradients are created causing ions and electrons to diffuse from the plasma to the sheath region. The presence of the probe causes a perturbation in both plasma density and potential in it's vicinity. In this case the plasma parameters determined from the probe characteristic are not the same as those of the undisturbed plasma.

This problem has been attacked theoretically by various researchers[2-7]. In general they make the following assumptions:

(1) The plasmas are diffusion controlled.

(2) Electrons have a Maxwellian energy distribution.

(3) A priori assumption of a space charge sheath of finite thickness on the probe at potentials other than plasma potential.

The next step in the analysis is generally to choose a reasonable model for the disturbance of the plasma in the neighborhood of the probe. This model depends upon the range of probe size and gas pressure considered. Common to most models is the space charge sheath and a diffusion controlled presheath. The presheath being defined

as a region in which $n_i = n_e \neq n_o$.

The mathematical treatment of the problem consists of the matching of particle currents at the boundaries of these sheaths to satisfy the condition of continuity of current. The boundary conditions vary depending upon individual assumptions.

Results consist of various methods by which true values of the plasma parameters can be determined from an analysis of the experimental data acquired when Langmuir's conditions are violated.

The only experimental work that has been done in regard to the perturbation problem is that of T. Okuda and K. Yamamoto[16]. Although not applied to a specific theory, their results indicate qualitatively what most of these theories predict.

This work is an attempt to establish experimentally the validity of one of these theories. This theory is that of Waymouth[6] which, after an examination of Langmuir's original theory in Section II, is presented in Section III.

The experiment consists of examining the plasma disturbance caused by a large probe for which Langmuir's assumptions do not hold, with a small probe for which Langmuir's conditions are valid. Results are compared to the predictions of Waymouth's theory.

II Langmuir Probe Theory

This section presents the theoretical interpretation of Langmuir probe theory for an ideal probe in the positive column of a gas discharge. A plane probe is considered first, then the spherical probe modification is discussed since it is directly applicable to both probes used in this experiment.

A. Assumptions

Make the following assumptions:

(1) The only particles in the positive column are electrons, positive ions and neutral gas molecules.

(2) There is electrical neutrality.

(3) The electrons and ions each possess a Maxwellian velocity distribution with different temperatures.

(4) The mean free paths of all plasma particles are large with respect to probe dimensions.

B. Positive Probe

When the probe potential V_s is made positive with respect to plasma potential (V_p in Fig. 1), ions are repelled and saturation electron current is drawn in the probe circuit. If the positive column has a density of n_o electrons per cubic meter with an average random velocity of v_e, then the electron current density leaving the cloud is $\frac{1}{4} n_o v_e$, from kinetic theory. If all of these electrons, reaching the probe at their normal rates of diffusion, contribute to the probe current, that is, do not return to the plasma, then electron saturation current is

$$I_e = \frac{1}{4} n e v_e A \text{ for } V_s > V_p \qquad \text{II-1}$$

where A is the surface area of the probe and $v_e = \sqrt{8eV_e/\pi m}$. V_e is the electron

temperature in volts and e and m the charge and mass of the electron respectively. This region of electron saturation is represented in the probe characteristic of Fig. 1 as the dotted line in region A.

C. Negative Probe

As probe potential is made negative with respect to plasma potential, the electrons encounter a retarding field. Only those electrons which have an energy such that the directed component of velocity $v_\perp$ normal to the plane of the probe surface fulfills the condition that $1/2\ m\ v_\perp^2 \geq e\ V_s$ where V_s is the difference of potential between plasma and probe or sheath potential, will contribute to the probe current. These electrons are given by the Boltzmann factor as

$$n = n_o e^{-V_s / V_e}$$

where n is the density of electrons at the probe surface when its potential is V_s lower than the plasma, and n_o is electron density in the undisturbed plasma. Electron current to the probe is then given by

$$I_e = n_o e A \sqrt{eV_e/2\pi m}\ e^{-V_s/V_e} \quad \text{for } V_F < V_S < V_P \qquad \text{II-2}$$

(Region B, Fig. 1)

As the probe is biased even more negative, a potential is reached at which the probe draws no current. This is equivalent to the potential acquired by an open circuit probe immersed in the plasma and is called the floating potential, V_F. Since electron random current is much greater than that of the ions, the probe becomes negatively charged to repel the electrons until both currents are equal.

As probe current is made still more negative, electron current decreases rapidly and is soon negligible. The probe draws only ion saturation current which is given by

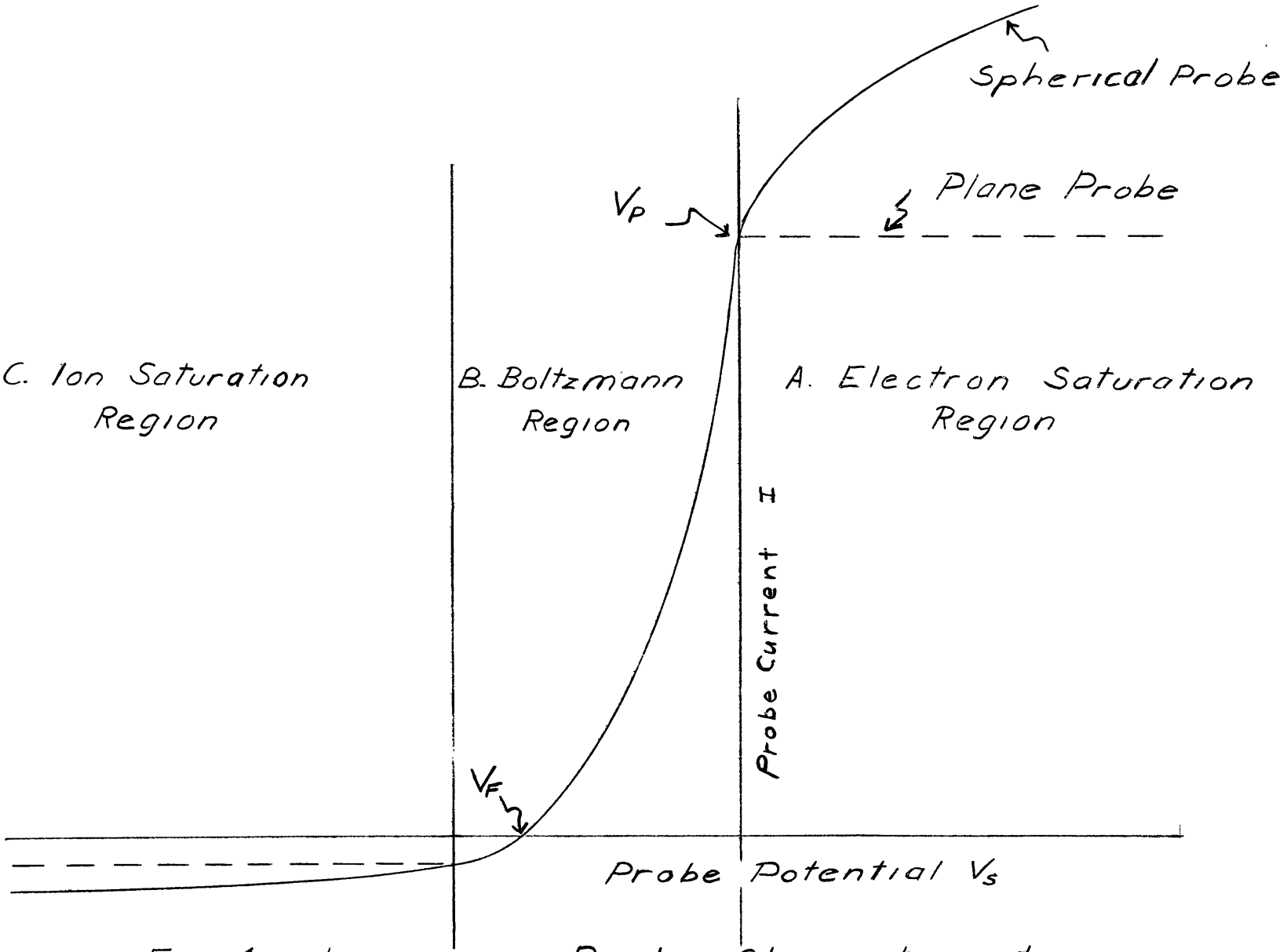

Fig. 1. Langmuir Probe Characteristic.

$$I_i = n_o e \frac{v_i}{4} A \text{ (Region C, Fig. 1)}$$

There is also a Boltzmann region for ion current which occurs when probe potential becomes slighly positive with respect to plasma potential. This results only in a slight bending of the knee since electron current is much greater than ion current. A comparison for saturation current values in the discharge used in this experiment is $I_e/I_i \sim 600$.

Total electron current is determined by correcting the resultant current for the ion current contribution. This is found by extrapolating ion saturation current to plasma potential.

D. Spherical Probe

The mechanism for charged particle collection by a spherical probe remains essentially the same as that described above with the exception that a correction must be made for changing sheath thickness. Increasing probe voltage increases sheath thickness which effectively increases probe area. Langmuir[8] showed that probe current for this case is given by

$$I = \left(\frac{n_o e v_e}{4}\right) 4\pi a^2 \left[1 - \frac{a^2 - r^2}{a^2} e^{-\frac{V_s r^2}{V_e (a^2 - r^2)}}\right] \quad \text{for } \frac{V_s}{V_e} > 0$$

and

II-3

$$I = (n_o e v_e/4)\, 4\pi r^2 e\, V_s/V_e \qquad \text{for } V_s/V_e < 0$$

where r is probe radius and a is sheath radius and is equal to the probe radius plus the Debye length. The solid line in Region A of Fig. 1 represents this correction.

E. Discharge Parameters

The probe characteristic can be made to give various important parameters of

the discharge. The methods for determining the parameters required by this experiment are discussed here.

It can be seen from equations II-1 and II-2 that a semilog plot of I vs. V_s yields a straight line in the Boltzmann region which breaks off at the plasma potential "knee". Electron temperature can be calculated from the slope of this straight line as

$$\ell n\ I_e = V_s/V_e + \text{constant}$$

or

$$V_e = \Delta V_s / \Delta \ell n\ I_e$$

Electron density can be determined from the value of the electron current at the plasma potential knee with a knowledge of probe area and electron temperature as

$$n_o = I_e/eA\sqrt{2\pi m/eV_e}\ ,$$

Referring to equations II-3, the values of these parameters are not effected by changing effective probe area due to changing sheath size.

III Waymouth's Theory[6]

When the mean free paths of plasma particles are of the order of or greater than probe dimensions, Langmuir probe theory no longer gives a valid interpretation of the plasma. Density gradients are set up causing ions and electrons to diffuse to the sheath region and the probe's electric field to penetrate the plasma beyond the sheath edge.

Waymouth treats the perturbation as a problem in ambipolar diffusion. His perturbation model consists of a free fall space-charge sheath and a diffusion controlled presheath.

The following assumptions are made:

(1) The plasmas are those of diffusion controlled discharges.

(2) Electrons have a Maxwellian energy distribution; electron and ion temperatures are independent of position and are unchanged by the presence of the probe.

(3) The probe radius is much smaller than tube radius, which insures that the losses of electrons and ions to the probe are small in comparison with diffusion losses to the walls. This is necessary if electron temperature is to be unchanged by the presence of the probe.

(4) Ion mobility is negligible in comparison to electron mobility.

(5) Probe radius is comparable to or greater than the mean free paths of plasma particles and is much greater than sheath thickness. Alternatively, the outer radius of the sheath is essentially the same as the probe. Sheath thickness is small in comparison to mean free paths.

The validity of this experiment in regard to these assumptions will be examined later.

The mathematics of Waymouth's theory consist of matching diffusion current from the plasma to random current across the sheath toward the probe. The problem is treated

in spherical coordinates as one dimensional and is outlined below. For mathematical details, refer to Waymouth's paper.

A. Perturbation of Electron Density

Begin with the transport equations:

$$\Gamma_e = - n \mu_e E - \mu_e V_e \nabla \cdot n$$

$$\Gamma_i = + n \mu_i E - \mu_i V_i \nabla \cdot n \qquad \text{III-1}$$

Take the divergence of both sides, set $\nabla \cdot \Gamma_e = \nabla \cdot \Gamma_i = n \nu_i$, eliminate E between the two, and arrive at the ambipolar diffusion equation.

$$\nabla^2 n + n\nu_i / D_a = 0 \qquad \text{III-2}$$

where

$$D_a = \frac{\mu_e \mu_i (V_e + V_i)}{\mu_e + \mu_i} = \mu_i (V_e + V_i)$$

when $\mu_i \ll \mu_e$

Solve this equation subject to the boundary conditions at the probe of radius r_p centered at r = 0, and at the wall at r = R. At the probe we have

$$\Gamma_e (r_p) = -n_p \sqrt{eV_e/2\pi m_e}\ \epsilon_i = - n_p \mu_e E - \mu_e V_e\ dn/dr \mid r_p$$

$$\Gamma_i (r_p) = -n_p \sqrt{eV_i/2\pi m_i}\ \epsilon_i = n_p \mu_i E - \mu_i V_i\ dn/dr \mid r_p \qquad \text{III-3}$$

where

$$\epsilon_e = e^{V_s/V_e} \quad \text{for } V_s < 0; \qquad \epsilon_i = 1 \quad \text{for } V_s < 0$$

$$\epsilon_e = 1 \quad \text{for } V_s > 0; \qquad \epsilon_i = e^{-V_s/V_i} \quad \text{for } V_s > 0$$

The left hand side of Eq. 3 represents the current of electrons and ions across the sheath toward the probe, as determined by the potential difference V_s across the sheath and the plasma density at the sheath edge n_p. The right hand side represents the transport of electrons and ions out of the plasma to the sheath edge under the combined influence of density gradients and electric fields.

Eliminating E between the two equations we get

$$1/n_p \; dn/dr \; | \; r_p = Q_T/r_p \qquad \text{III-4}$$

where

$$Q_T = Q_e + Q_i \qquad \text{III-5}$$

$$Q_e = \frac{r_p}{\mu_e(V_e + V_i)} \sqrt{e V_e / 2\pi m_e} \; \epsilon_e \; ; \; Q_i = \frac{r_p}{\mu_i(V_e+V_i)} \sqrt{\frac{eV_i}{2\pi m_i}} \; \epsilon_i$$

The solution to (2) in spherical coordinates is

$$n = 1/x \; \{A \sin x + B \cos x\}$$

where

$$x = \sqrt{\nu_i / D_a} \cdot r$$

and

$$B/A = \frac{- Q_T \; x_p}{1 + Q_T}$$

assuming ν_i is not altered by the presence of the probe.

If probe radius is much smaller than tube radius the density in the perturbed plasma is

$$n = n_o \left\{ 1 - \frac{Q_T}{1+Q_T} \frac{x_p}{x} \right\} \qquad \text{III-6}$$

The density at the sheath edge which will be determined from Langmuir probe analysis is

$$n_p = \frac{n_o}{1+Q_T} \qquad \text{III-7}$$

B. Perturbation of Plasma Potential

To calculate the penetration of the probes' electric field into the plasma return to the transport equations, take the divergence of both sides, and solve for the divergence of n E Note that div Γ_e = div Γ_i.

$$\nabla \cdot (n E) = -\left(\frac{\mu_e V_e - \mu_i V_i}{\mu_i + \mu_e} \right) \nabla^2 n$$

Using the fact that $\mu_i \ll \mu_e$ and assuming that V_i will be comparable to or less than V_e, obtain

$$\nabla \cdot (nE) = - V_e \nabla^2 n$$

Integrating and solving for the electric field,

$$E_r = - V_e \frac{1}{n} \frac{dn}{dr} + \frac{Q_e(V_e+V_i)}{1+Q} r_p \frac{n_o}{nr^2}$$

In the unperturbed plasma, n $\approx$ a constant n_o, and E $\approx$0. Regarding the potential of the unperturbed plasma as a constant V_o and calling the potential of the plasma at the sheath boundary V_p, we have

$$V_o = V_p - \int_{r_p}^{\infty} E_r dr$$

or

$$V_p - V_o = \Delta V = \int_{r_p}^{\infty} E_r dr \qquad \text{III-8}$$

where ΔV is the perturbation of plasma potential at the sheath boundary caused by the presence of the probe. Waymouth shows that this becomes

$$\Delta V = [V_e - \frac{Q_e (V_e + V_i)}{Q}] \ln (1 + Q_T) \qquad \text{III-9}$$

The first term in III-9 is the Boltzmann term, resulting from the fact that the potential and electron density are related in thermal equilibrium according to $n \sim \exp (V_s/V_e)$. From this term the plasma potential is shifted negative by the presence of the probe. The second term is large only when Q_e is a large fraction of Q_T, which can happen only when sheath potential is slightly negative, zero, or positive. Then the electron current to the probe is large and the electric field in the plasma must be reduced from the thermal equilibrium value to permit the increased current to flow.

IV The Experiment

A. Discharge Tube

The experimental discharge tube is shown in the photograph of Fig. 2 and the diagram of Fig. 3. It is constructed of 120 mm I.D. pyrex tubing with a smaller tube attached at one end for movement of the small-probe with respect to the large-probe. It has both a cathode and an anode at each end for reversing the discharge.

The cathodes are the standard fluorescent-lamp type made of triply coiled tungsten wire with a tri-oxide coating to enhance electron emmission.

The anodes are stainless steel which have the area of their inner edges increased by means of stainless steel rims from pipes which have been welded on and smoothed. This construction avoided the occurrence of "hot spots" which have been found to form on this edge in similar discharges.

The large-probe is a hollow copper sphere 0.515 cm. in diameter supported 20 mil ($\sim$0.5 mm) tungsten wire which is shielded by uranium glass. See Fig. 4.

The small-probe dimensions were kept as small as possible to satisfy Langmuir's conditions. Its construction, see Fig. 5, was similar to W. Verweij's[9]. The sensing element of the probe consists of a 2 mil ($\sim$ 0.05 mm) tungsten wire which has been "balled" (r $\sim$0.12 mm) with a small mercury arc welder. This geometry was chosen on the basis of the following considerations. A plane probe made from a glass coated wire would have an unknown and varying area due to electrical contact between liquid mercury occurring on the glass coating and the probe wire. A cylindrical probe would have made position less definitive. The position of the probe used is determined by a weighted fraction of the entire probe, that is, the cylindrical support wire and the spherical tip.

The probe enters a protective quartz tube of as small dimensions as was found possible ($\sim$0.2 mm O.D.). Within this tube, the probe wire is surrounded by a spacing

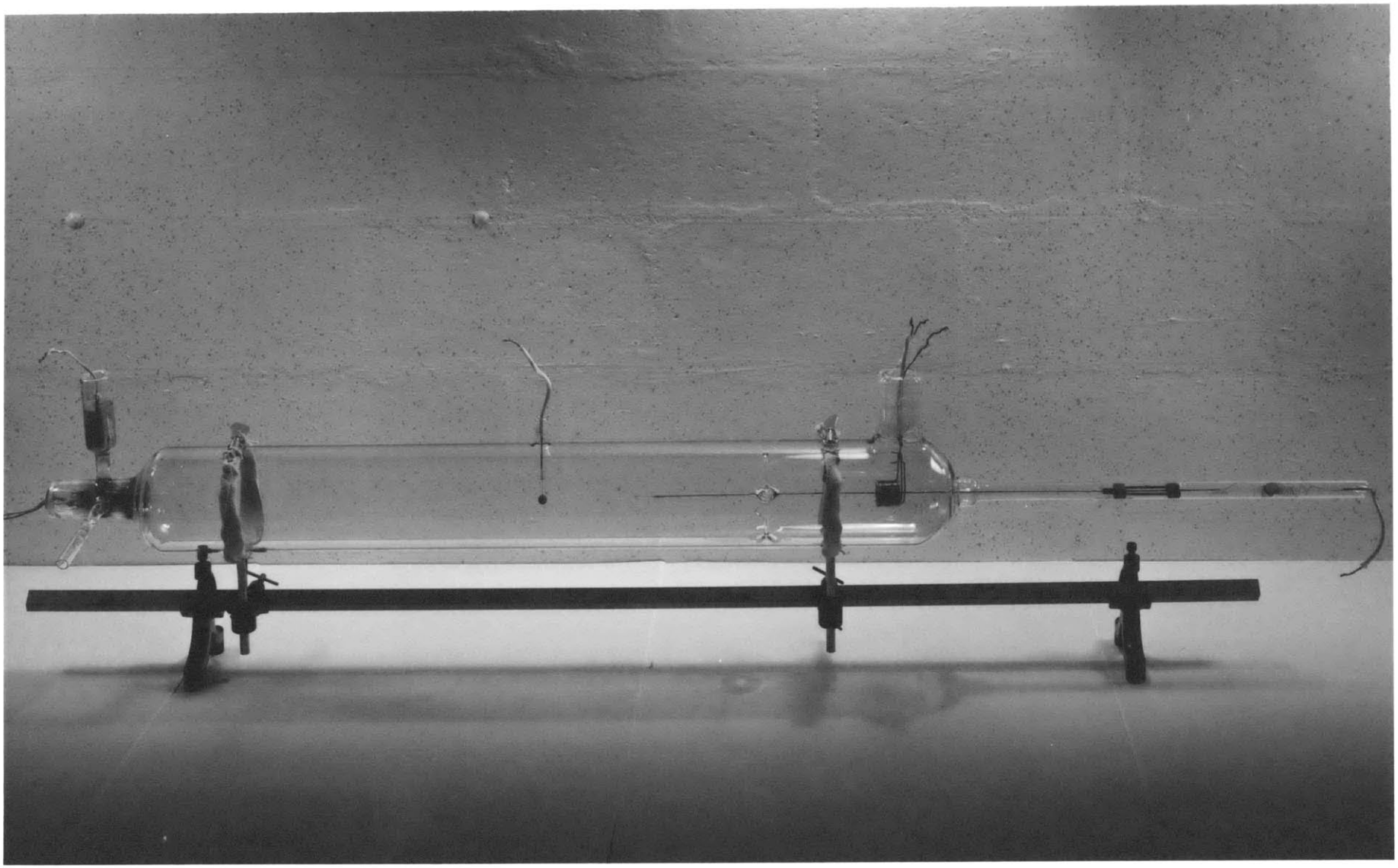

Figure 2 Photo of Discharge Tube

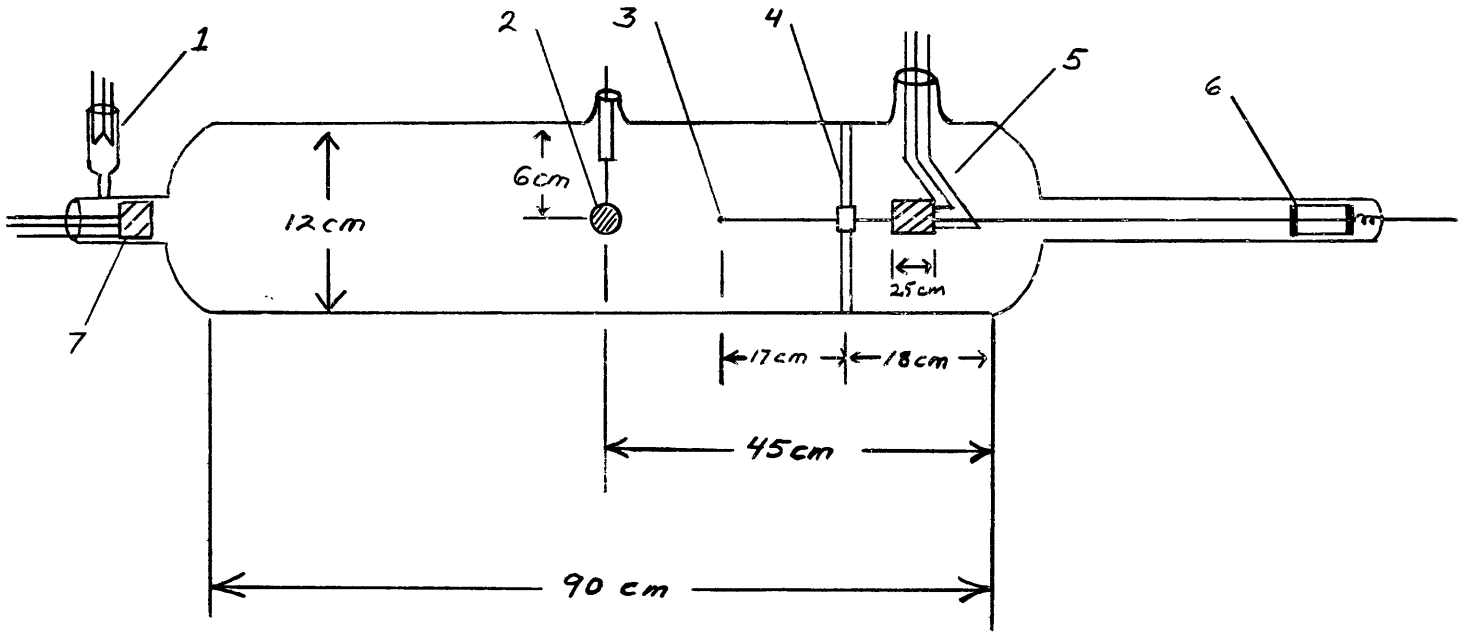

1.) Barium Getter
2.) Large Probe
3.) Small Probe
4.) Glass Spider
5.) Anode and Cathode
6.) Moveable Slug
7.) Anode and Cathode

Fig 3. Diagram of Discharge Tube

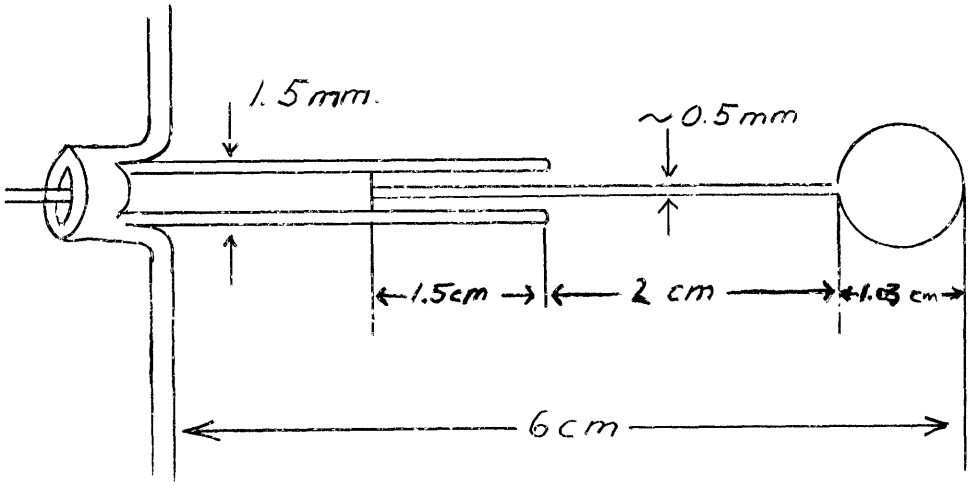

Fig. 4. Large Probe

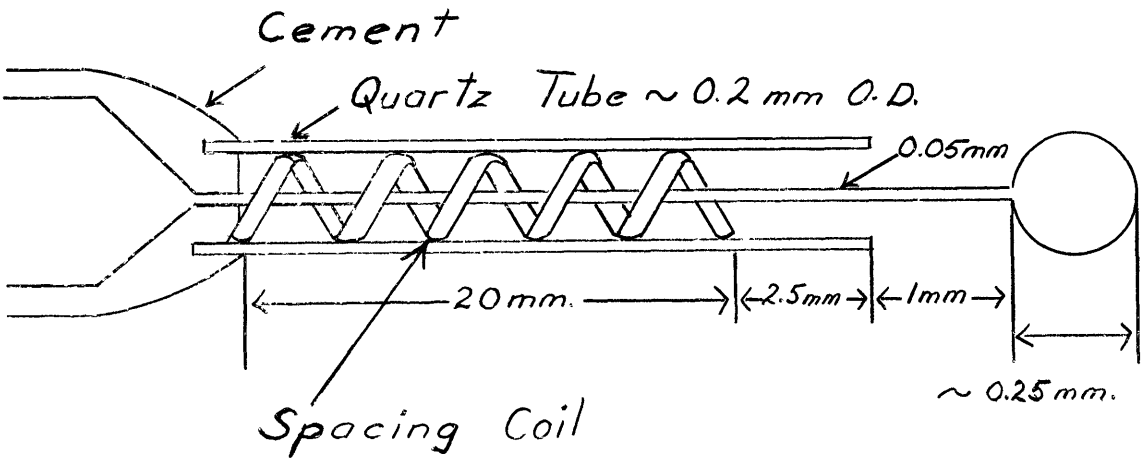

Fig. 5. Small Probe

coil to ensure that no electrical contact is made between the probe wire and any mercury that happened to condense on the quartz shield. The length of the probe wire exposed to the plasma is the result of a compromise between being long enough to avoid edge effects due to the space-charge layer on the quartz tube and yet short enough such that the area of the wire support was as small a fraction of the sphere area as possible (~ 0.7) for definition of location. This probe cannot be seen in the photograph, only its shield.

The tiny probe wire and protective quartz sleeve are attached to a larger pyrex insulated tungsten wire (30 mil ~ 0.75 mm) which with the help of the glass "spider" spans the distance from a moveable slug in the tubular arm to measuring positions near the large probe. This support wire is attached to the moveable iron slug by a Kovar joint. The probe current is carried to the press by a loose coil. The axial position of the small probe can be varied by sliding the iron slug with a solenoidal magnet. This sliding mechanism, designed by T. Fohl[10], allowed small-probe positions to be varied from $r \sim 0.53$ cm to $r \sim 10.3$ cm where $r = 0$ corresponds to the center of the large probe ($r_p = 0.515$).

It can be seen from Fig. 3 that the small-probe support wire passes through the anode necessarily close to the cathode. To prevent the heated cathode from melting the wire's glass insulation, a molybdenum heat shield was attached between support wire and cathode.

The discharge tube also contained a barium getter to ensure the purity of the gas contents.

The tube was processed according to the schedule in Appendix I and filled with spectroscopically pure He to a pressure of 1 mm Hg ($\pm 5\%$), liquid mercury was also added.

B Waymouth's Conditions Satisfied

Waymouth's theory of Section III imposes the following requirements on the

discharge tube.

$$R \gg r_p \gg \lambda_e \gg r_s$$

where

R = tube radius

r_p = large-probe radius

λ_e = mean free path of electrons

r_s = small-probe radius

These conditions are satisfied reasonably well as

60 mm $\gg$ 5.15 mm $\gg$ 0.6 mm $\gg$ .12 mm

Waymouth's theory also requires that sheath size be less than mean free path. A calculation, for very positive probe potentials, using Langmuir's parallel plate space-charge equation shows that maximum sheath size is < 0.4 mm (see Appendix II).

The small probe perturbation parameter Q_T (calculation of perturbation parameters will be discussed later) is ~ 0.10 which indicates that applying Langmuir's theory to this probe is a good approximation.

C. Probe Measurement Technique

Probe contamination is a serious problem in acquiring Langmuir probe curves. These effects have been found [11] in mercury arcs due to mercury condensing on the probe when it is cool and evaporating when hot. This contamination changes the probe work function and causes an inaccurate determination of probe voltage. Probe work function can be stabilized in either of two ways, by heating the probe with electron bombardment which evaporates the Hg film, or by ion bombardment which causes a film of liquid mercury to be built up on the probe, thus presenting a uniform potential to the plasma. In both cases, probe curves are taken immediately after stabilizing the work function either by a point by point method or a pulse method. In this experiment ion bombardment was used with a pulse technique.

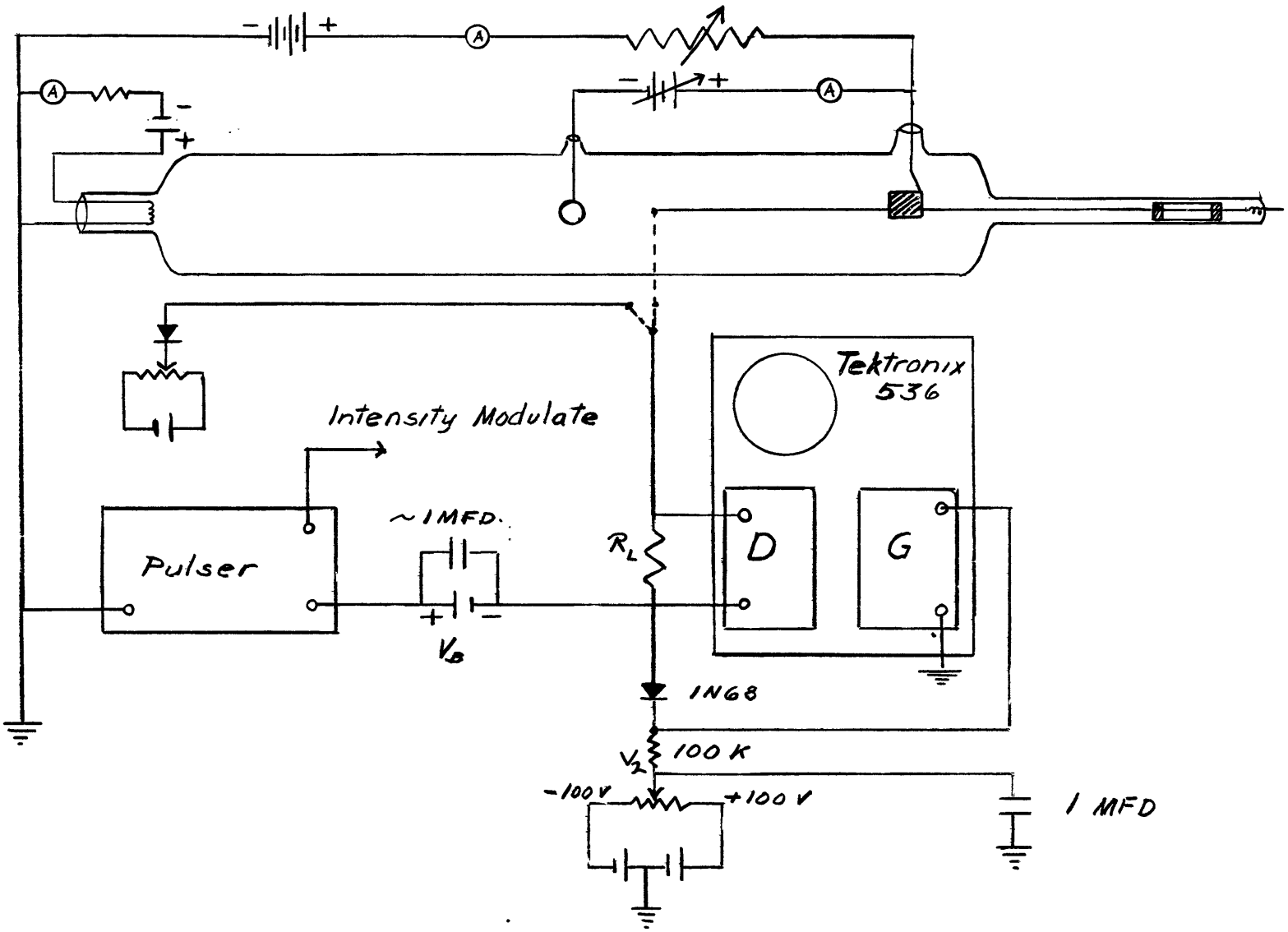

Fig 6. Circuit Diagram

The pulse technique [12] consists of maintaining the probe at a negative potential with respect to the plasma except when it is pulsed positive. As a result of the negative biasing the work function on the probe remains essentially constant. During the pulse, which carries the probe potential positive with respect to the plasma, the current voltage characteristic is recorded by an oscilloscope. The circuit diagram is shown in Fig. 6. The negative bias on the probe is established by the bias voltage V_b. Pulse repitition rate is 60 cps while pulse amplitude can be varied. The probe current is measured by the drop across resistance R_L. In order to stay in the linear region of the oscilloscope horizontal amplifier, only the portion of the pulse exceeding an adjustable bias V_2 is fed to the horizontal input. The voltage drop across R_L is fed to the vertical input. The current-voltage curve on the oscilloscope is then photographed. Voltages have to be corrected for the voltage drop across the measuring resistance R_L. A Type 536 Textronix oscilloscope was used with a Type G plug-in unit for the horizontal signal and a Type D (because of its high rejection ratio) plug-in unit for the vertical signal. Details of the pulser construction can be found in Ref. 12.

To establish a reference voltage on the oscilloscope trace, a diode, biased at the same potential as the measured floating potential, was pulsed alternately with the probe by manual switching. The diode characteristic, superimposed upon the probe characteristic by doubly exposed photographs, established the floating potential as a reference. A typical probe curve with reference can be seen in the photograph of Fig. 7.

D. Sequence of Measurements

To keep the noise level at a minimum, the discharge tube, including filaments, was operated solely on dc power in the form of storage battery banks. Since either cathode or anode oscillations show up prominently on the oscilloscope trace in the measuring technique used, the tube was, in a sense, continuously monitored. All

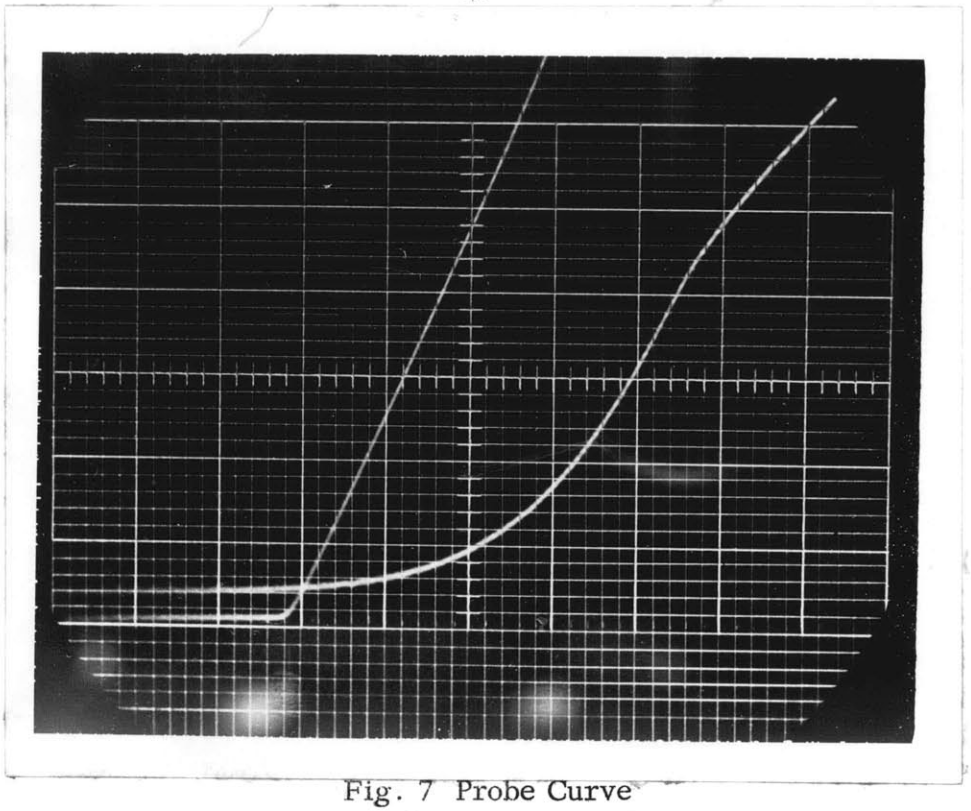

Fig. 7 Probe Curve

small-probe curves were taken with the cathode potential as a reference while the large-probe was biased from the anode (See Fig. 6).

Two data taking methods were used: (a) Current to the large-probe was kept constant while small-probe curves were taken as a function of distance from the large-probe. Large-probe bias was changed and the steps were repeated. (b) Small-probe position was kept constant while small-probe curves were taken as a function of large-probe potential. Small-probe position was changed and the steps were repeated. The close agreement of the two methods established the stability of the discharge.

Since the large-probe drew considerable current (~0.1 amperes maximum), a constant current of 0.6 amperes was maintained on the side of the discharge tube from which small-probe data was being taken. This required ballast resistance adjustments for data taken on the electron downstream side of the large-probe.

Large-probe data was acquired by a point by point method. Although no cleaning precautions were taken, large-probe curves showed little hysteresis. Curves from various runs also correlated well.

E. Method of Determining Parameters

Electron densities relative to the undisturbed plasma (the density determined at the point of farthest withdrawal of the small-probe) were determined from the knee of the photographed I-V curves with an error of less than 5%. The floating potential of the small-probe was determined with a Keithley 610 A electrometer. An identical electrometer was used to measure large probe voltages. Plasma potential was determined from the diode reference characteristic and the probe curve knee with an error of less than 5%. Electron temperature could be calculated from the slope of the semi-log current voltage plot taken from the photographs, (error ~10%). The position of the small-probe was measured with respect to the large-probe with a Cenco measuring microscope and was accurate to within 1%.

F. Waymouth-Bitter Theory[13]

Applying the Waymouth-Bitter theory of fluorescent lamp analysis to the discharge predicts an electron temperature of 10,800° and an axial electric field of 130 volts/meter. Although the electron temperature prediction correlates well with experimental results, the electric field is ~25% lower than was observed. This could be due to the rather large diameter of the discharge tube which may require modifications in theory as is indicated in their paper.

V Experimental Results Compared to Theory

A. The Method

A comparison of the experimental results to the predictions of Waymouth's theory is made in the following way:

1. On the basis of the gas pressure of the discharge tube, the radius of the large-probe, and the electron temperature, the electron and ion perturbation parameters, Q_e and Q_i, are calculated from equations III-5 as a function of the unknown ion temperature. Electron temperature is determined from the slope of the semi-log plot of the large-probe curve, since it approaches a straight line at negative probe potentials. Large-probe curves are then constructed for various ion temperatures using Waymouth's equations for the density and potential perturbations (equations III-6 and III-9). The constructed curve which best fits the experimental large-probe curve establishes the ion temperature which in turn establishes Q_e and Q_i. This first set of Q values is then a result of calculations based on Waymouth's theory. The only experimental data used is V_e and V_i both determined from the large-probe curve.

2. Small-probe density data, taken as a function of distance from the large-probe, can be made to yield Q_T. Equations III-5 show that for potentials less than plasma potential, Q_i is constant and $Q_e \sim \exp\ V_s/V_e$. Therefore, by varying the large-probe voltage in this region, Q_T can be varied. At potentials near floating potential $Q_e \approx 0$ and $Q_T \approx Q_i$, so that all the Q values can be established experimentally from the small-probe data. Data taken on the electron upstream or cathode side of the large-probe will be referred to as cathode-side data while data taken on the electron downstream or anode side of the large-probe will be referred to as anode-side data.

3. The calculated Q's are then compared to the experimentally determined Q's.

4. The potential perturbation is estimated from small-probe data and compared to the calculated potential perturbation.

B. Calculated Q's

Q_i can be calculated as a function of V_i from equation III-5 which is

$$Q_i = \frac{r_p}{\mu_i (V_e + V_i)} \sqrt{\frac{eV_i}{2\pi m_i}} \epsilon_i \qquad \text{(V-1)}$$

V_e is the electron temperature (0.87 ev) determined from the slope of the straight line portion of the large probe semilog plot. Hg_+ mobility, μ_i, in He (p= 1 mmHg) and Hg vapor (p=0.01 mmHg) was determined as 0.82 m^2/volt-sec on the basis of experimental data from L. M. Chanin and M.A.Biondi[14] and F. R. Kovar[15]. Biondi's measurements were essentially for Hg_+ in pure He since his mobility tube was cool (~27°C) and his helium pressures were high (p >6 mm Hg). Kovar's zero field mobility for Hg_+ in Hg vapor was combined with Biondi's using Blanc's Law to arrive at the resultant mobility.

Based upon this data, Q_i becomes

$$Q_i = \frac{1.72\, V_i^{1/2}}{0.87 + V_i} \epsilon_i \qquad \text{(V-2)}$$

To determine Q_e as a function of V_i, Eq. III-5 is reduced to a more convenient form using the following substitutions,

$$\mu = e/m\nu_c, \quad \nu_c = pP_c\, v_e$$

$$v_e = \sqrt{8eV_e/\pi m}, \text{ and } \lambda_e = 1/pP_c$$

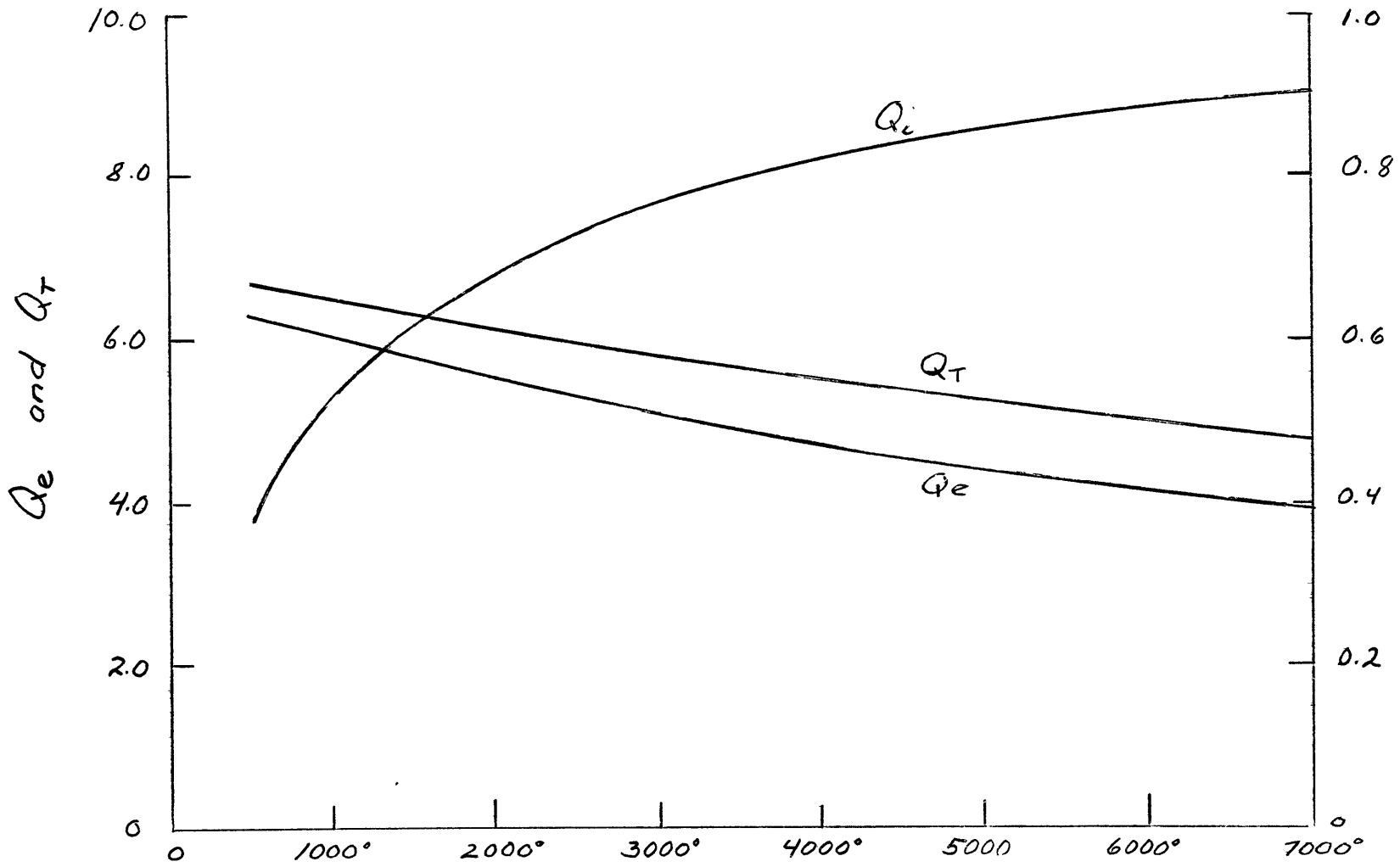

Fig 8. Q_e, Q_i and Q_T vs. T_i

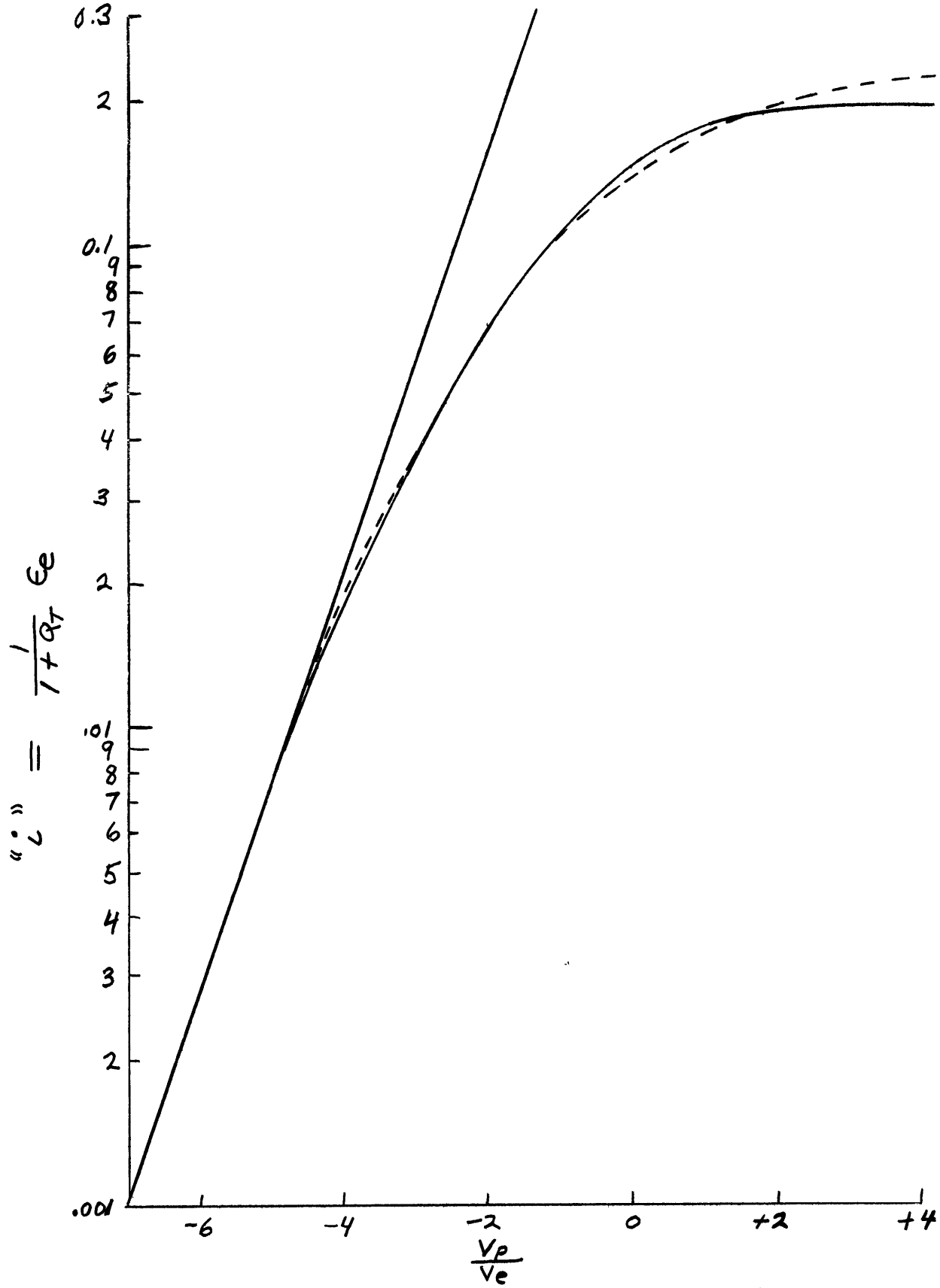

Fig 9. Large Probe Curve Best Fit : Cathode-side

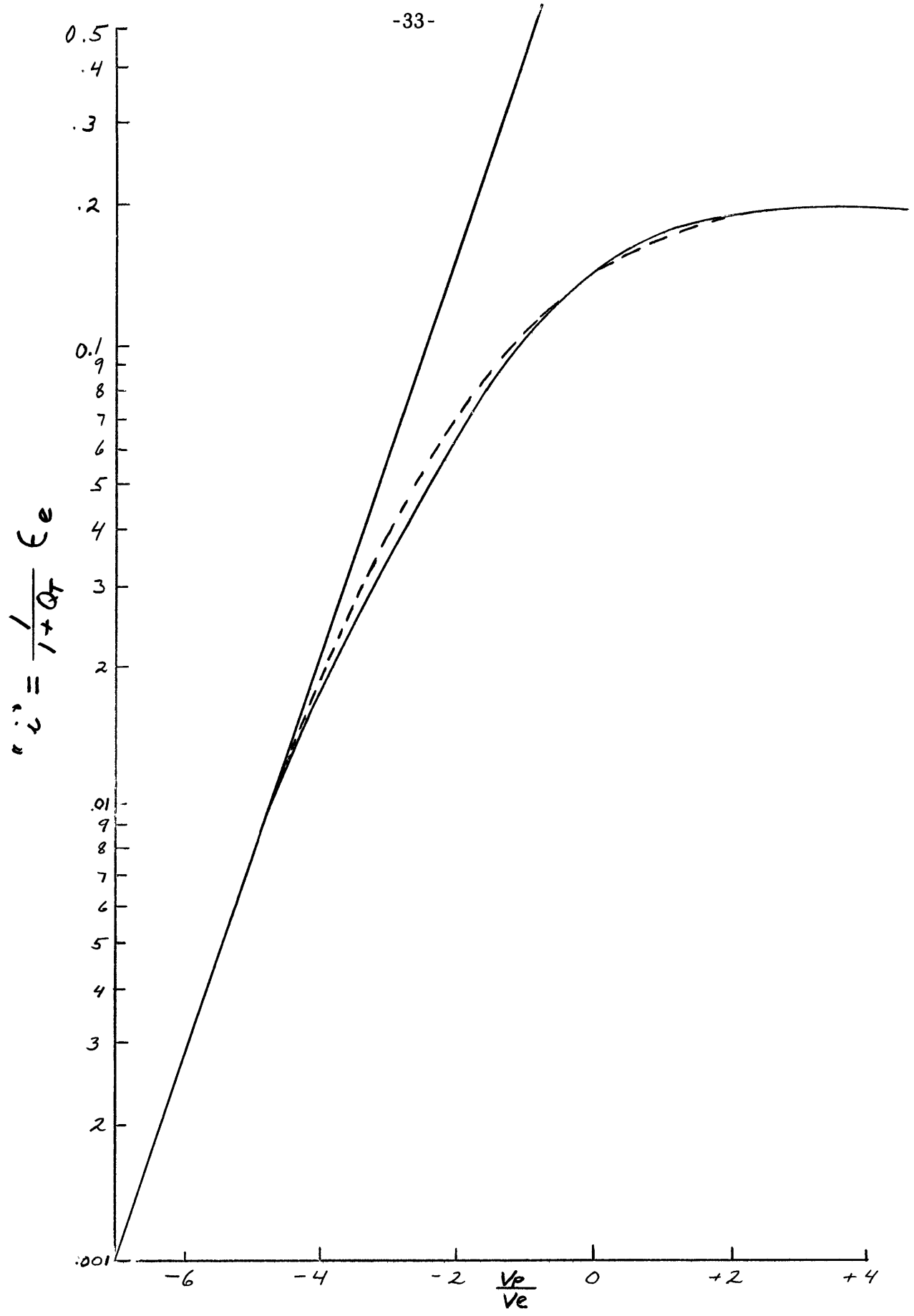

Fig. 10. Large-Probe Curve Best Fit: Anode Side

where ν_c and P_c are electron collision frequency and probability, respectively. III-5 becomes

$$Q_e = \left(\frac{r_p}{\lambda_e}\right)\left(\frac{V_e}{V_e + V_i}\right)\left(\frac{3}{2\pi}\right)^{1/2} \epsilon_e$$

or

$$Q_e = \frac{5.83}{0.87 + V_i}\,\epsilon_e$$

Q_e, Q_i, and $Q_T = Q_e + Q_i$ are plotted in Fig. 8 for $\epsilon_e = \epsilon_i = 1$. Note that as V_i increases, Q_i increases, Q_e decreases, and Q_T decreases.

For an assumed V_i, a large-probe curve can be calculated as a function of the potential of the plasma at the sheath boundary, V_P, on the basis of this data. The best fit to the experimental data establishes V_i. See App. III for constructed best fit.

Experimental large-probe curves determined when small-probe data was taken on the cathode-side and the anode-side of the discharge tube are shown as the dotted lines of Fig. 9 and 10, respectively. The solid lines represent the calculated best fit. The calculated curve for $V_i = 2/3\ V_e$ could be used for both fits since the experimental curves differ only slightly, in the electron saturation region. This difference may be the result of discharge current adjustments which were necessary for anode-side data. This fit then establishes V_i which in turn establishes the calculated Q values .

C. Small-probe Q Determinations

The Q parameters can be established experimentally from small-probe density data. Q_T is determined from the slope of the plot of $1-n/n_o$ vs. r_p/r since from Eq. III-6,

$$1 - \frac{n}{n_o} = \frac{Q_T}{1 + Q_T}\,\frac{r_p}{r}$$

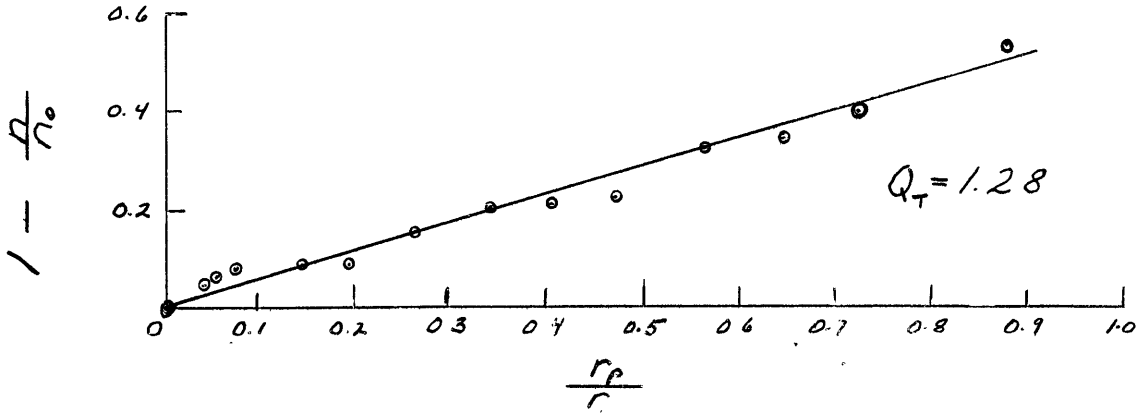

Fig. 11. Large Probe Current = 1.1 ma

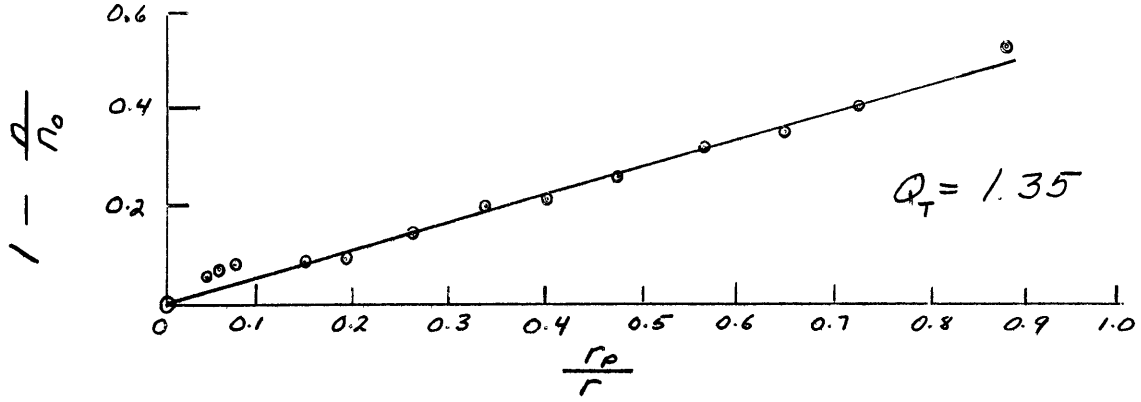

Fig 12. LPI = 3.5 ma.

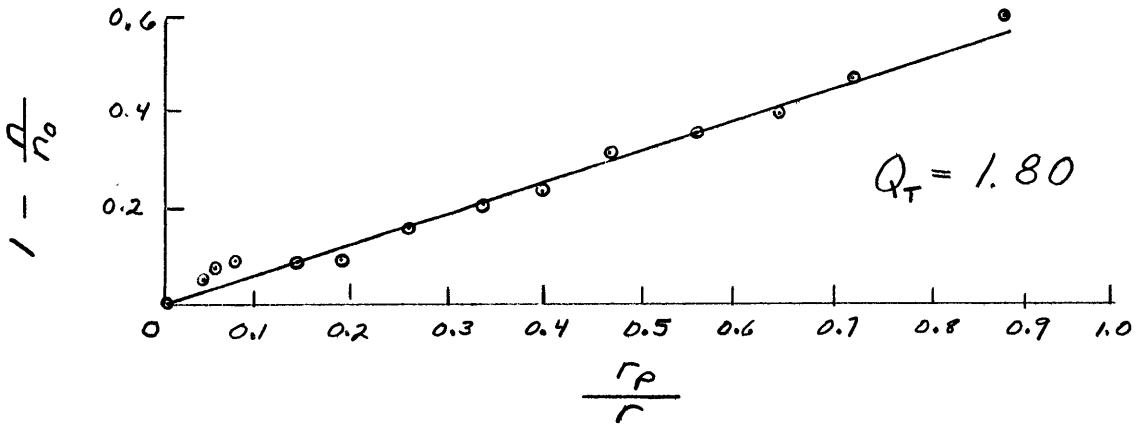

Fig 13. LPI = 11.3

(Cathode-Side Data)

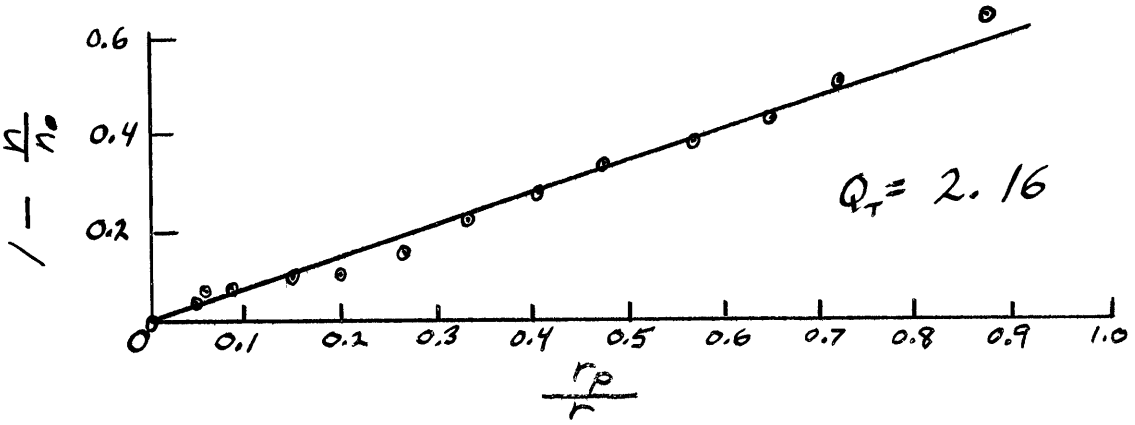

Fig. 14. Large Probe Current = 18.9 ma

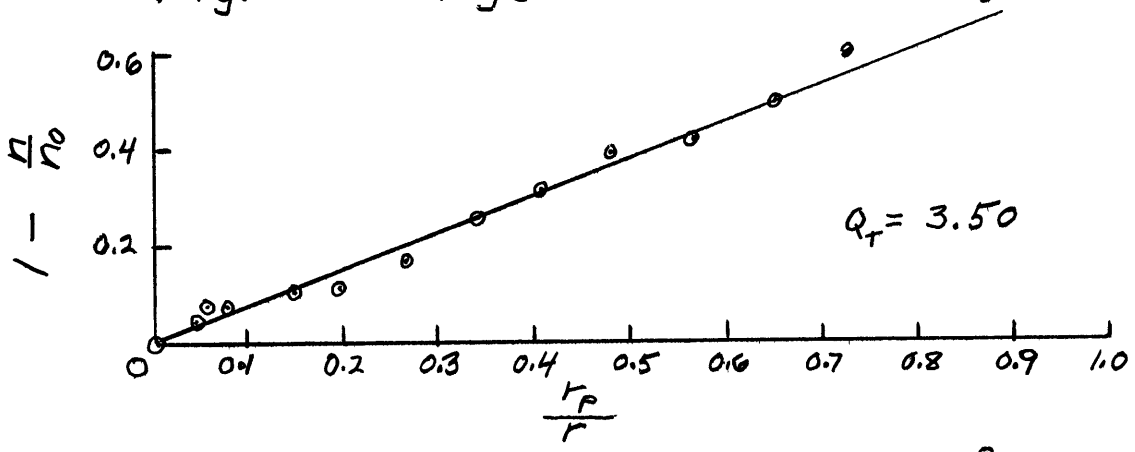

Fig. 15. LPI = 40.9 mq.

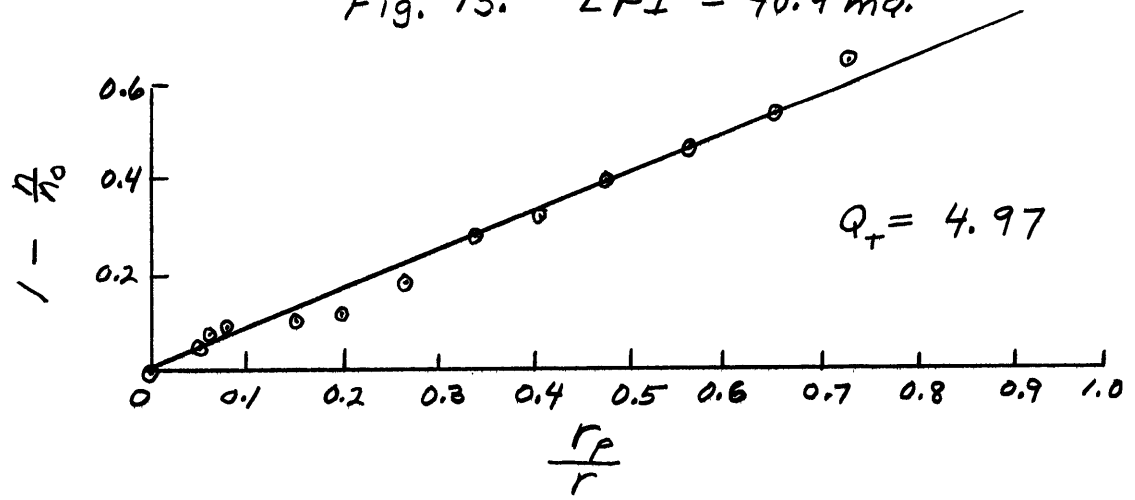

Fig. 16. LPI = 76.9 mq.

(Cathode-Side Data)

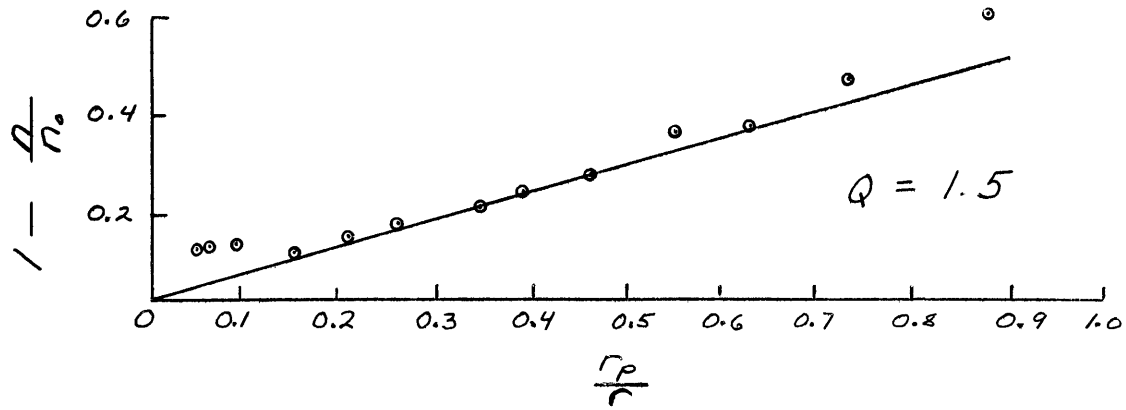

Fig. 17. Large Probe Current = 1.1ma.

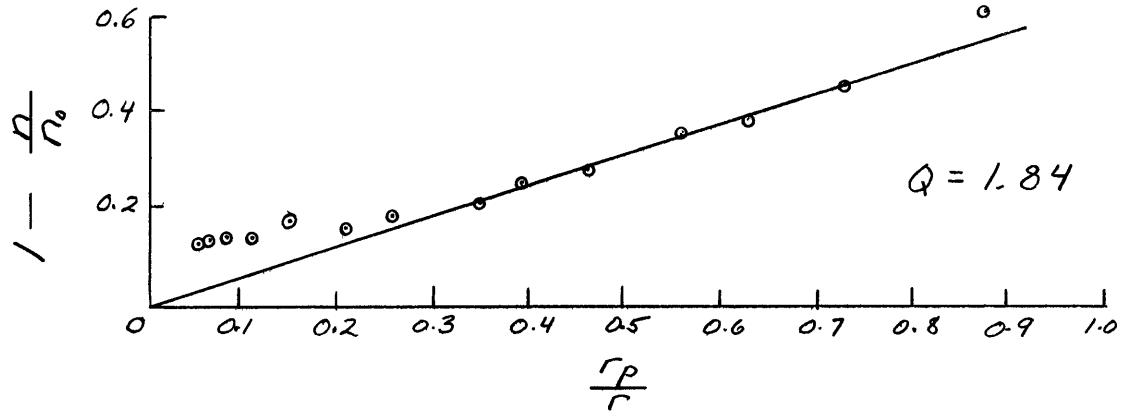

Fig. 18. LPI = 3.5ma.

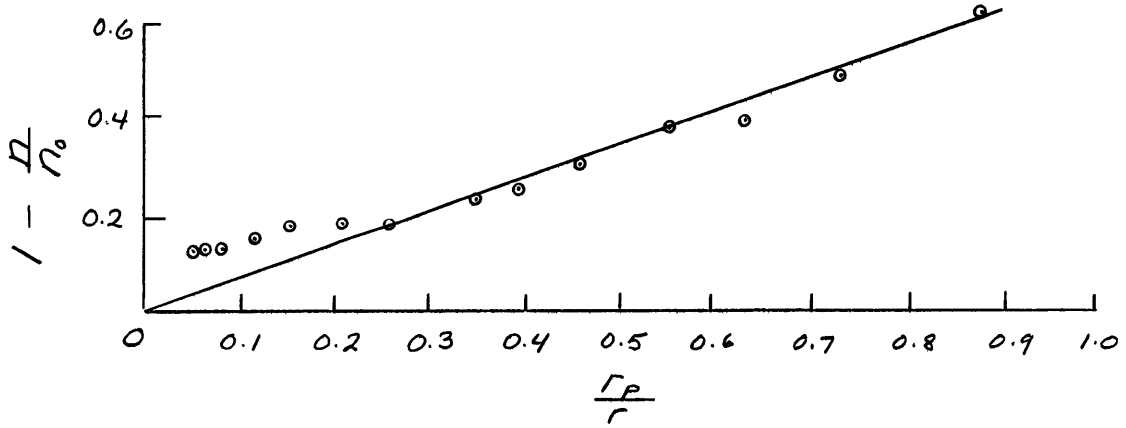

Fig. 19. LPI = 11.3 ma.

(Anode-Side Data)

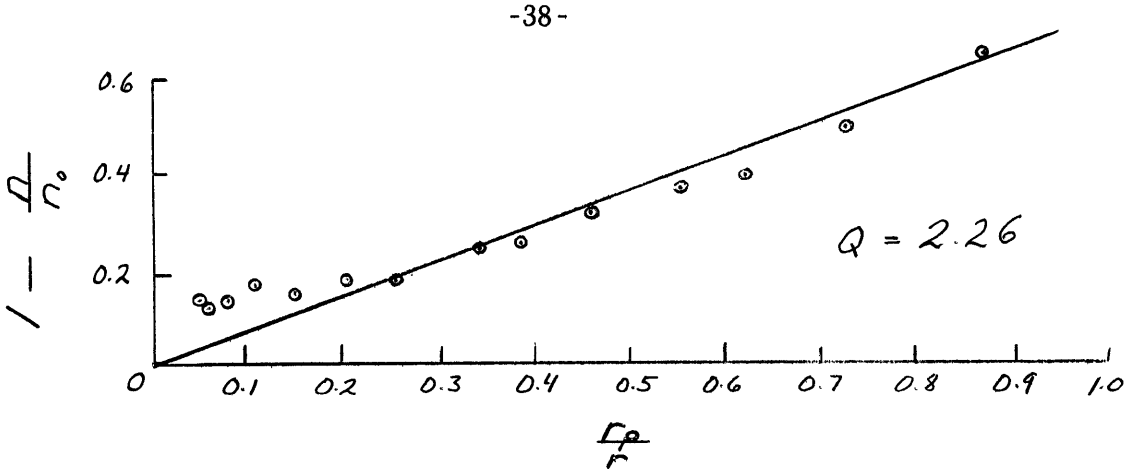

Fig. 20. Large Probe Current = 18.9 ma.

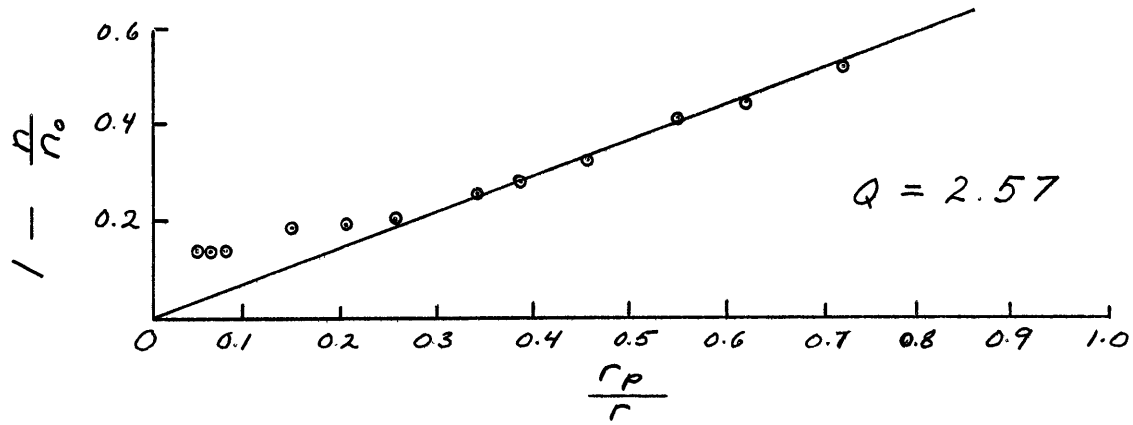

Fig. 21. LPI = 40.9 ma.

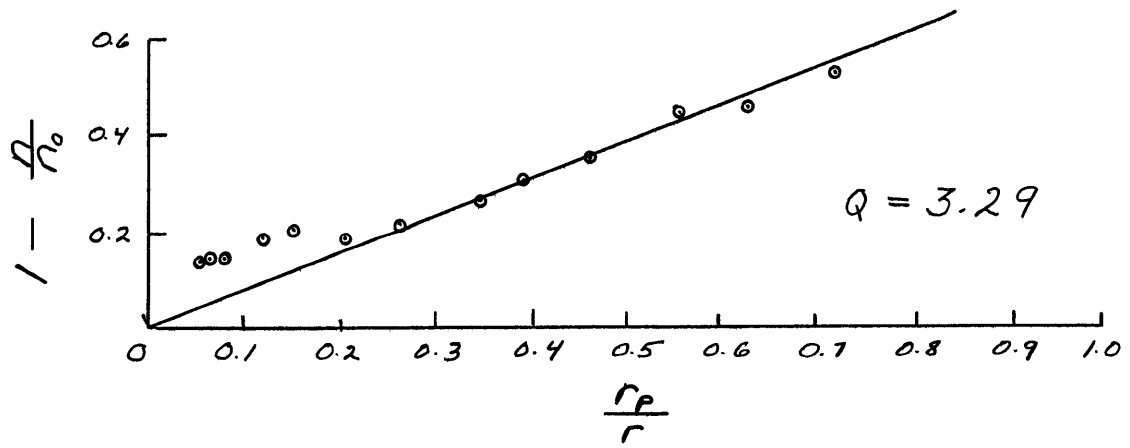

Fig 22. LPI = 70.9 ma.

(Anode-Side Data)

Figs. 11-16 and 17-22 show these plots for cathode- and anode-side data, respectively. These Q_T's are determined for six different large-probe voltages since varying large probe voltage varies Q_e, which varies Q_T.

Although the last point appears to be consistantly off, cathode-side data gives evidence to the 1/r density dependence predicted by the theory. This is not necessarily true of data taken on the anode side of the large-probe. Although a straight line has been fitted to the points, definite curvature exists.

D. The Comparison

Figs. 23 and 24 illustrate the comparison between calculated and experimental Q's for cathode- and anode-side data, respectively. The abscissas represent the large-probe sheath voltage ($V_S = V_P - \Delta V$) determined by the curve fit and normalized to the electron temperature. Curves A represent experimental large-probe current; curves B are the calculated Q_T's upon which the constructed large-probe curve was based; and curves C are the Q_T's determined from small-probe data. V_s for the small-probe data points was determined by correlating the large probe currents with the constructed best fit voltages and removing the ΔV component.

As has been discussed, for large probe potential near floating potential $Q_T \approx Q_i$ which is a constant. This was verified experimentally since Q_T for very negative potentials was found to be the same as the floating potential Q_T determination. The Q_i determined in this way can be subtracted from the Q_T values at less negative potentials to determine Q_e as a function of V_s. A semi-log plot of Q_e vs. V_s should yield a straight line the slope of which corresponds to the electron temperature since

$$Q_e = Q_{eo} \epsilon_e = Q_{eo} e^{-V_s/V_e}$$

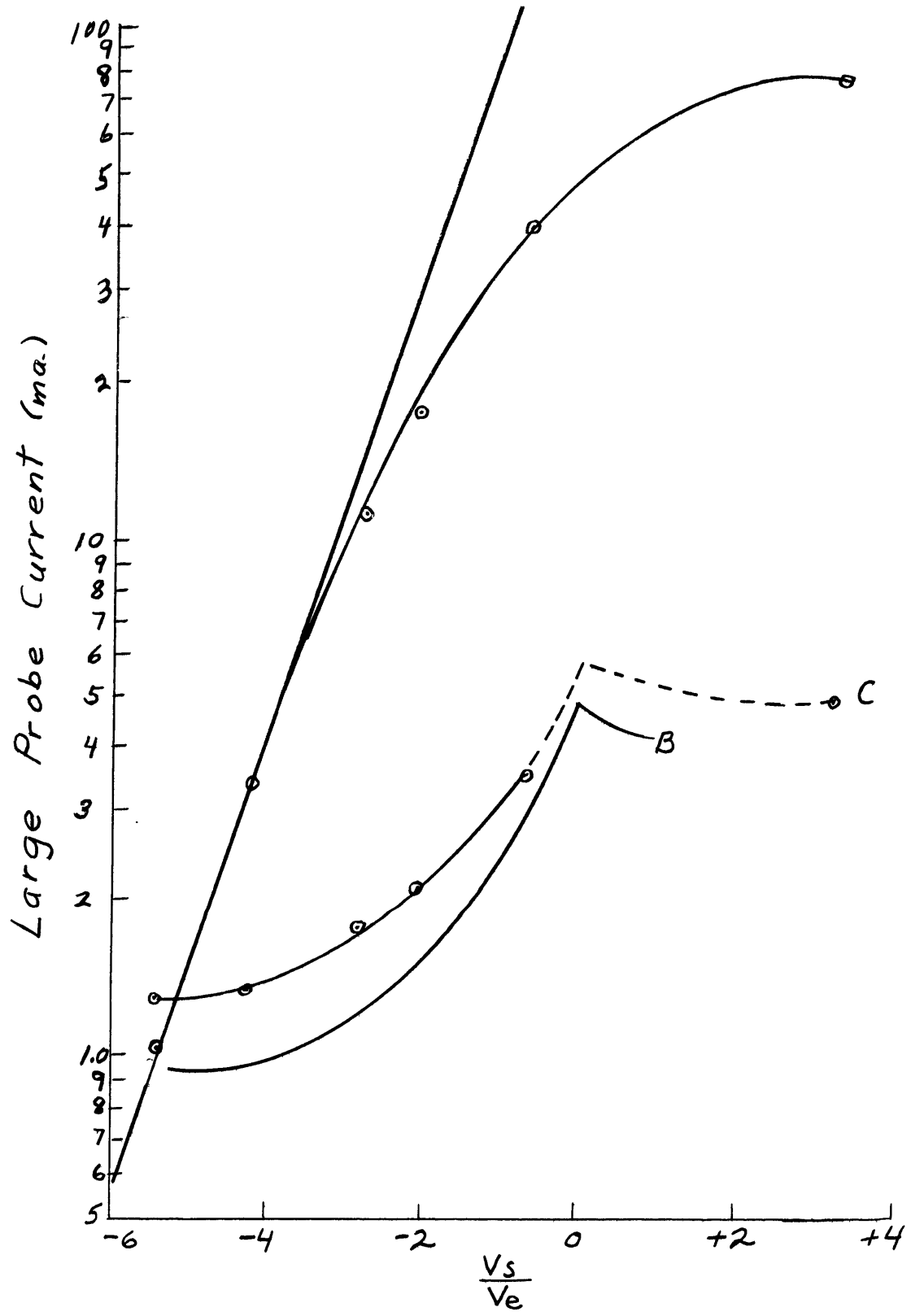

Fig. 23. Comparison : Cathode – Side

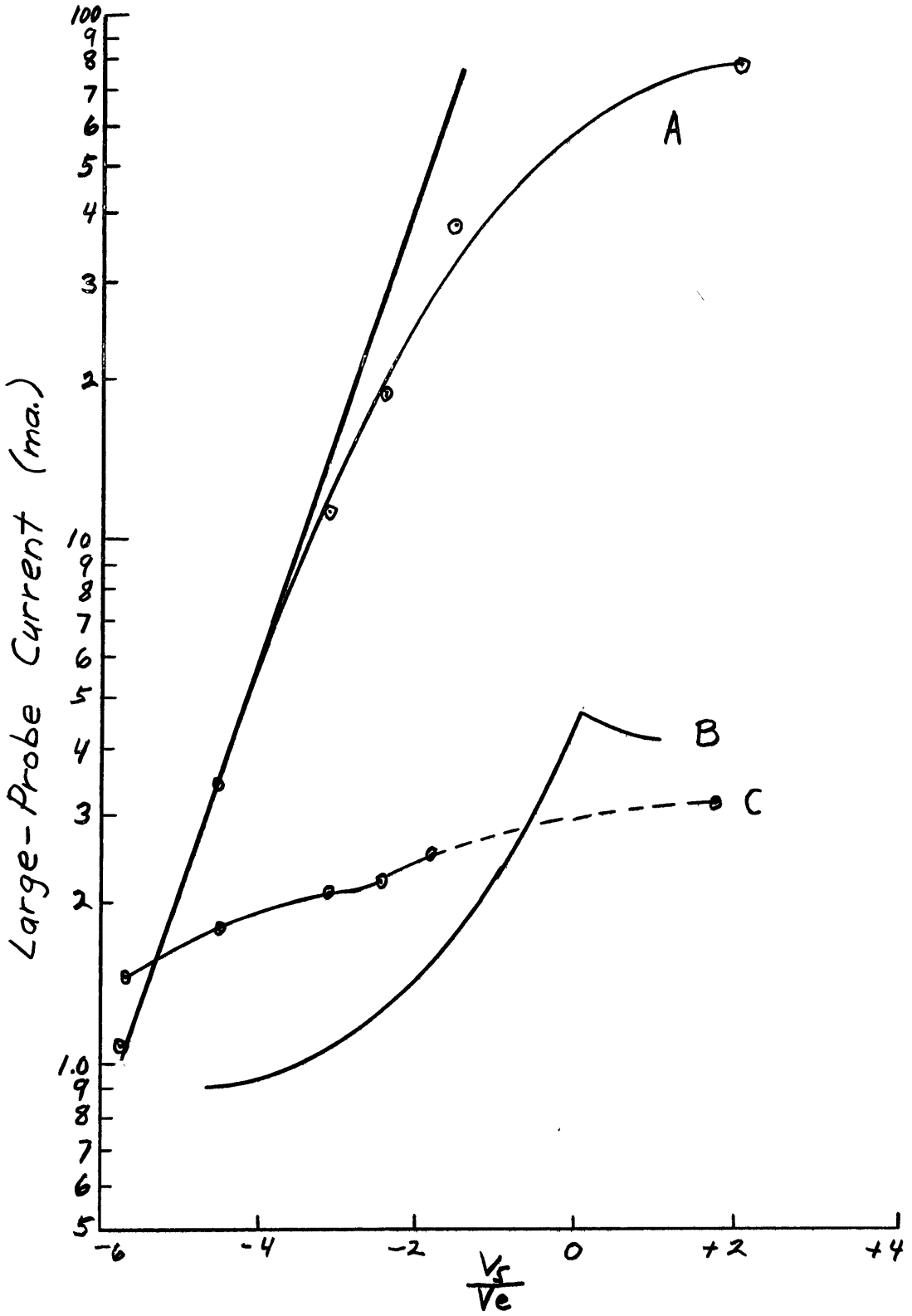

Fig. 24. Comparison: Anode Side

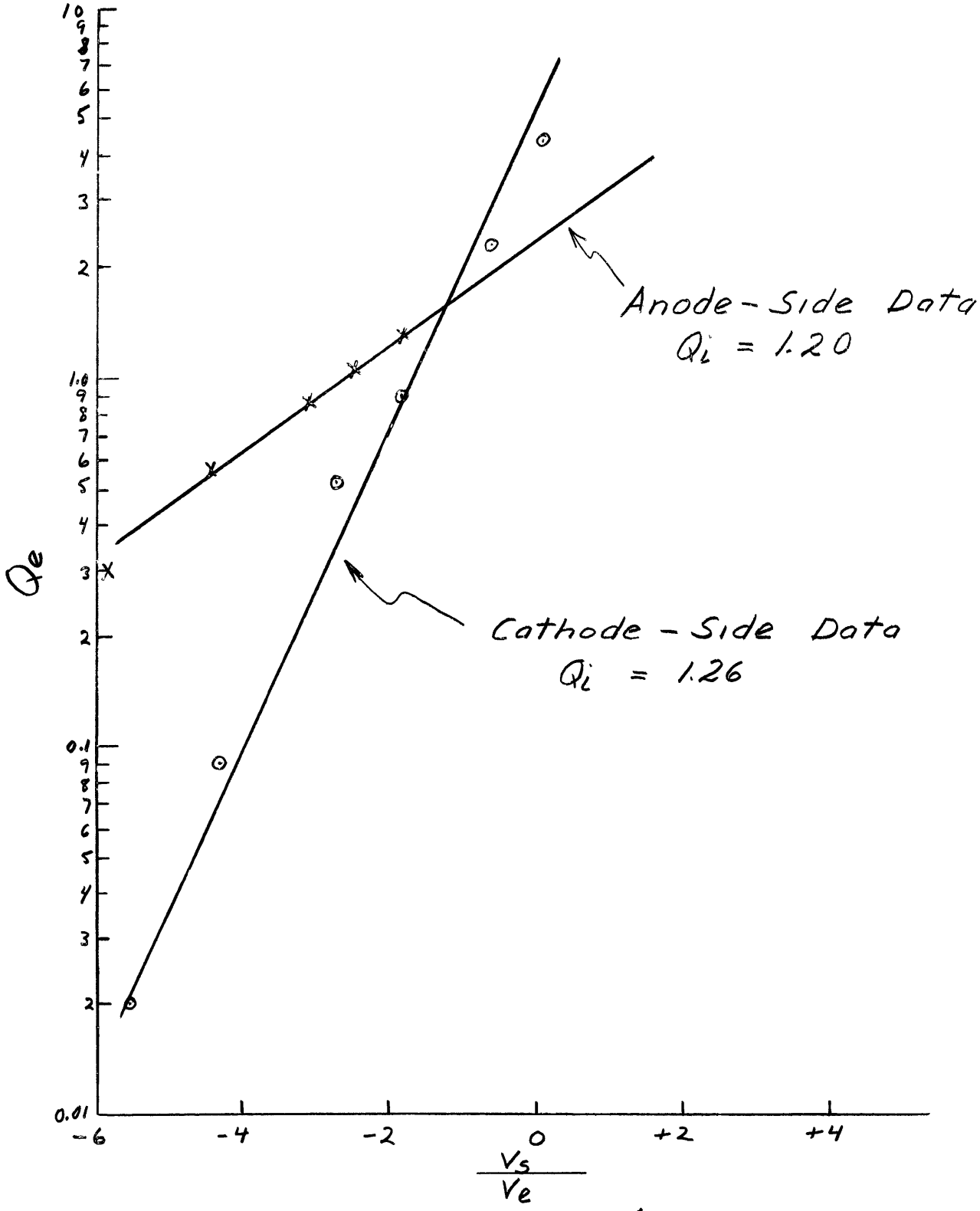

Fig 25. Qe vs. $\frac{V_s}{V_e}$

or

$$\ell n Q_e = V_s/V_e + \text{constant}$$

so that

$$V_e = \Delta V_s / \Delta \ell n Q_e$$

Q_{eo} is the value of Q_e when $\epsilon = 1$ or $V_s \geq 0$. Since all voltages are normalized in this analysis, the slope should correspond to 1 ev. Curves A and B of Fig. 25 represent these plots for cathode- and anode-side data, respectively.

Summarizing, cathode-side data of Fig. 23 shows good correspondence between small-probe Q_T and curve fitting Q_T determinations. The slope of the straight line of curve A, Fig. 25, corresponds to an electron temperature of approximately 1 ev indicating that Q_e has the correct sheath voltage dependence. There is a discrepancy in this data, in that the small-probe Q_i determination is about 25% larger than the calculated Q_i.

Anode-side data of Fig. 24 shows that the small-probe Q_T determinations do not correlate well with those calculated. The slope of the straight line of curve B, Fig. 25, corresponds to a very high electron temperature.

E. The Potential Perturbation

From Eq. III-9, the theoretical potential perturbation, ΔV, is plotted as a function of sheath voltage (in Fig. 26). The perturbation is negative for potentials near floating potential, passes through zero, and becomes positive for potentials near plasma potential.

Figs. 27 and 28 are small-probe determinations of plasma potential as a function of r/r_p for various large probe voltages, cathode- and anode-side data, respectively. These curves are offset for clarity.

For cathode side determinations plasma potential is negative, passes through zero, and becomes positive for increasing large-probe voltages.

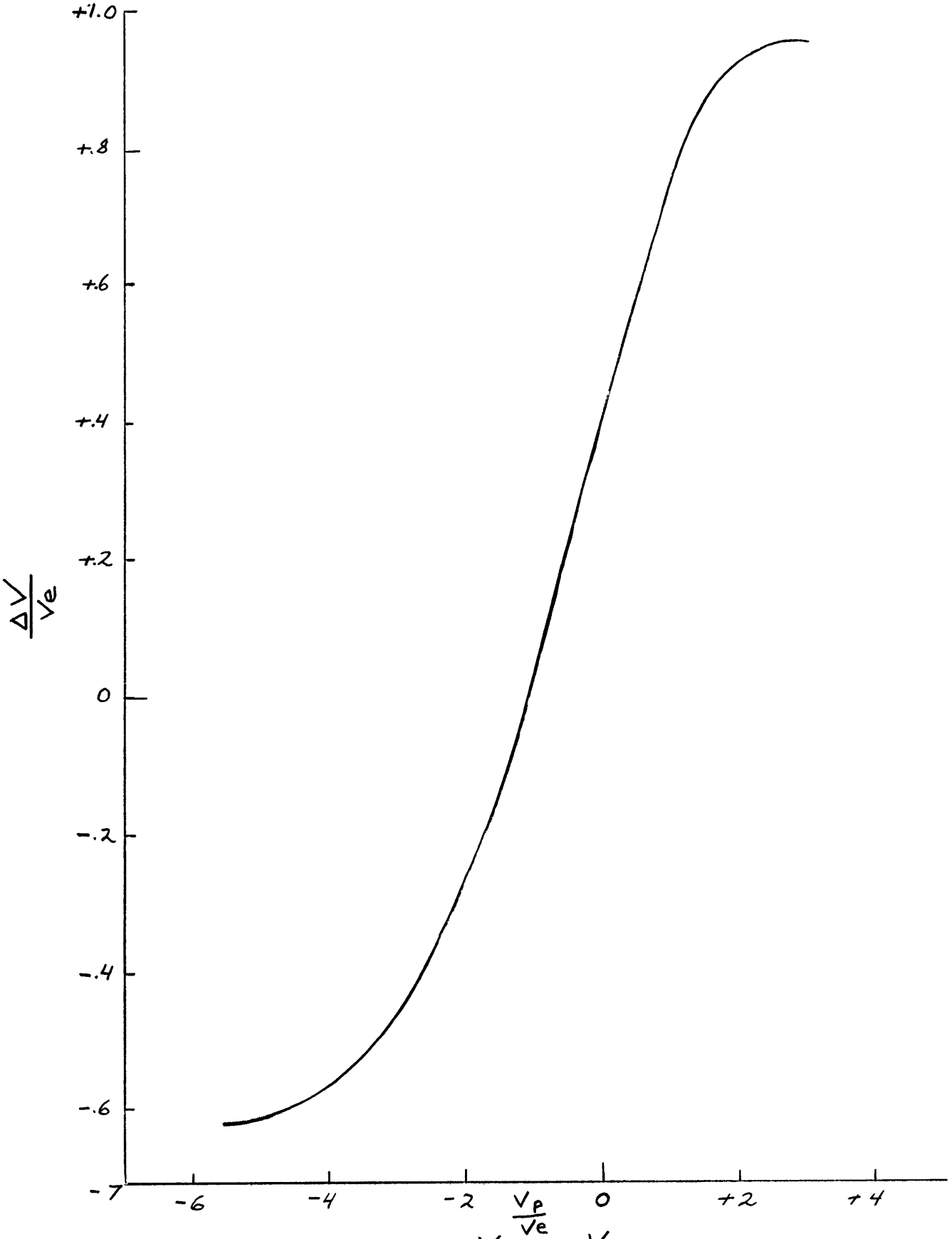

Fig 26. $\frac{\Delta V}{V_e}$ vs. $\frac{V_p}{V_e}$ (Calculated)

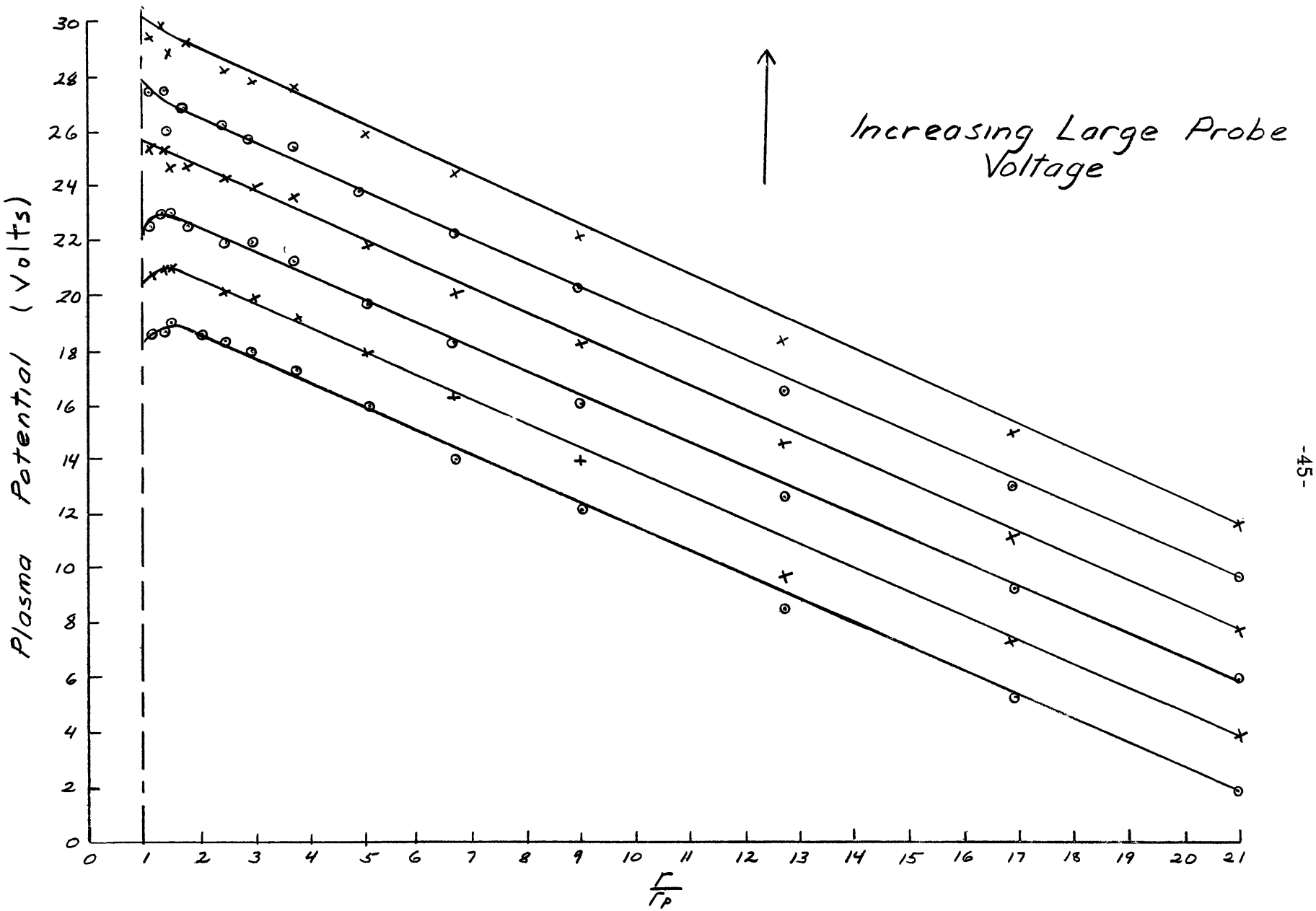

Fig. 27. Plasma Potential : Cathode-Side Data

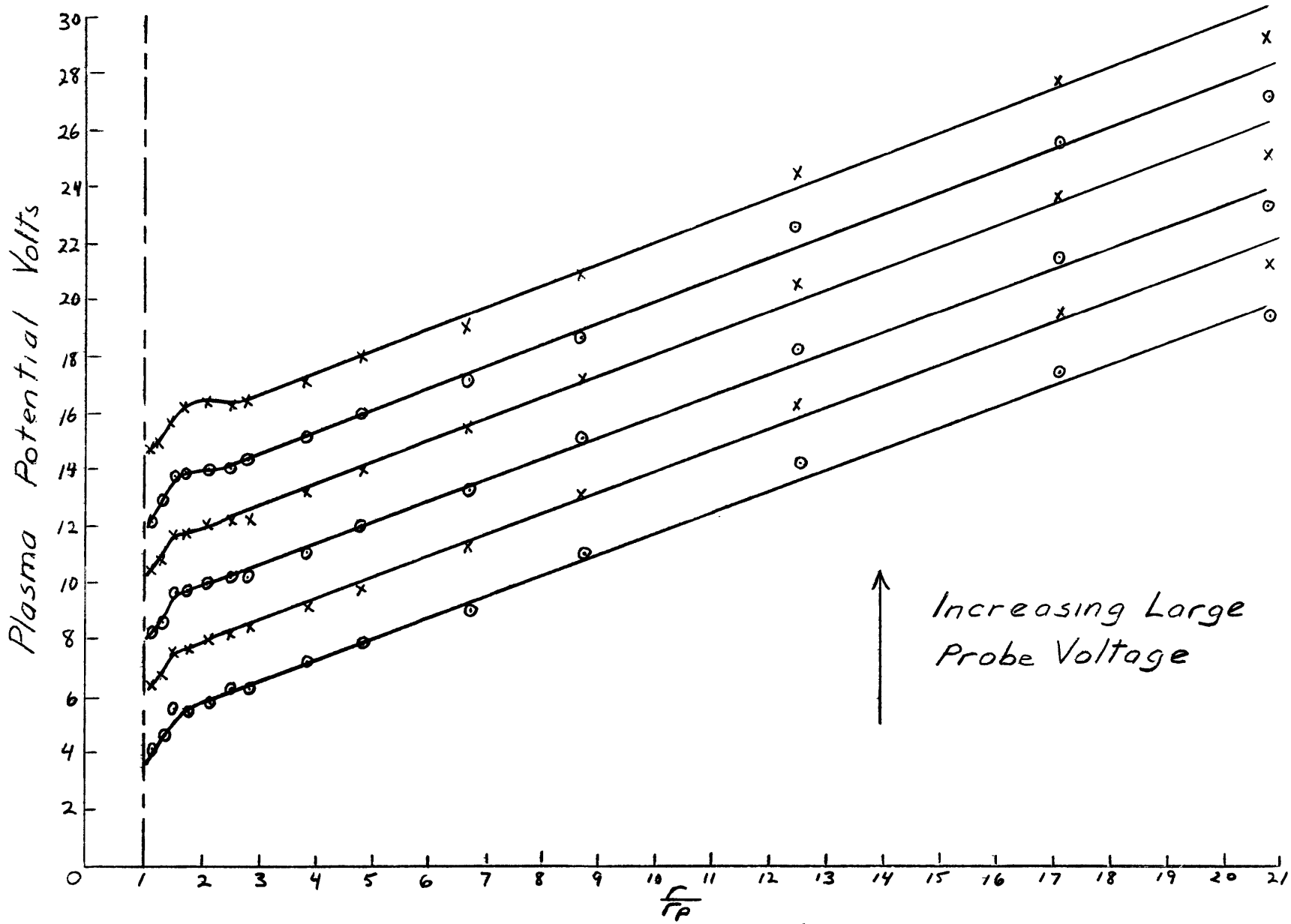

Fig. 28. Plasma Potential : Anode - Side Data.

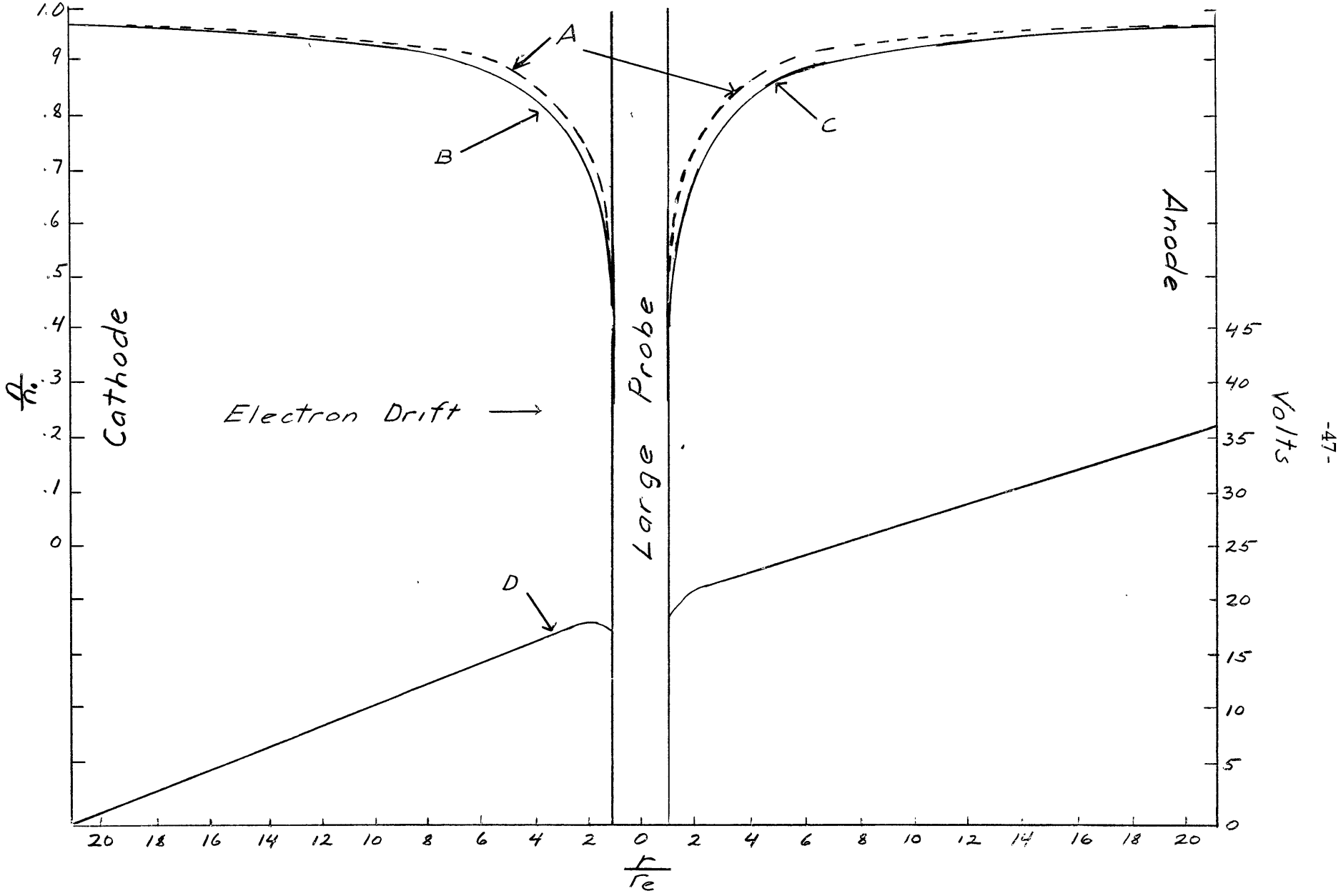

Fig. 29. Composite: Large Probe at Floating Potential

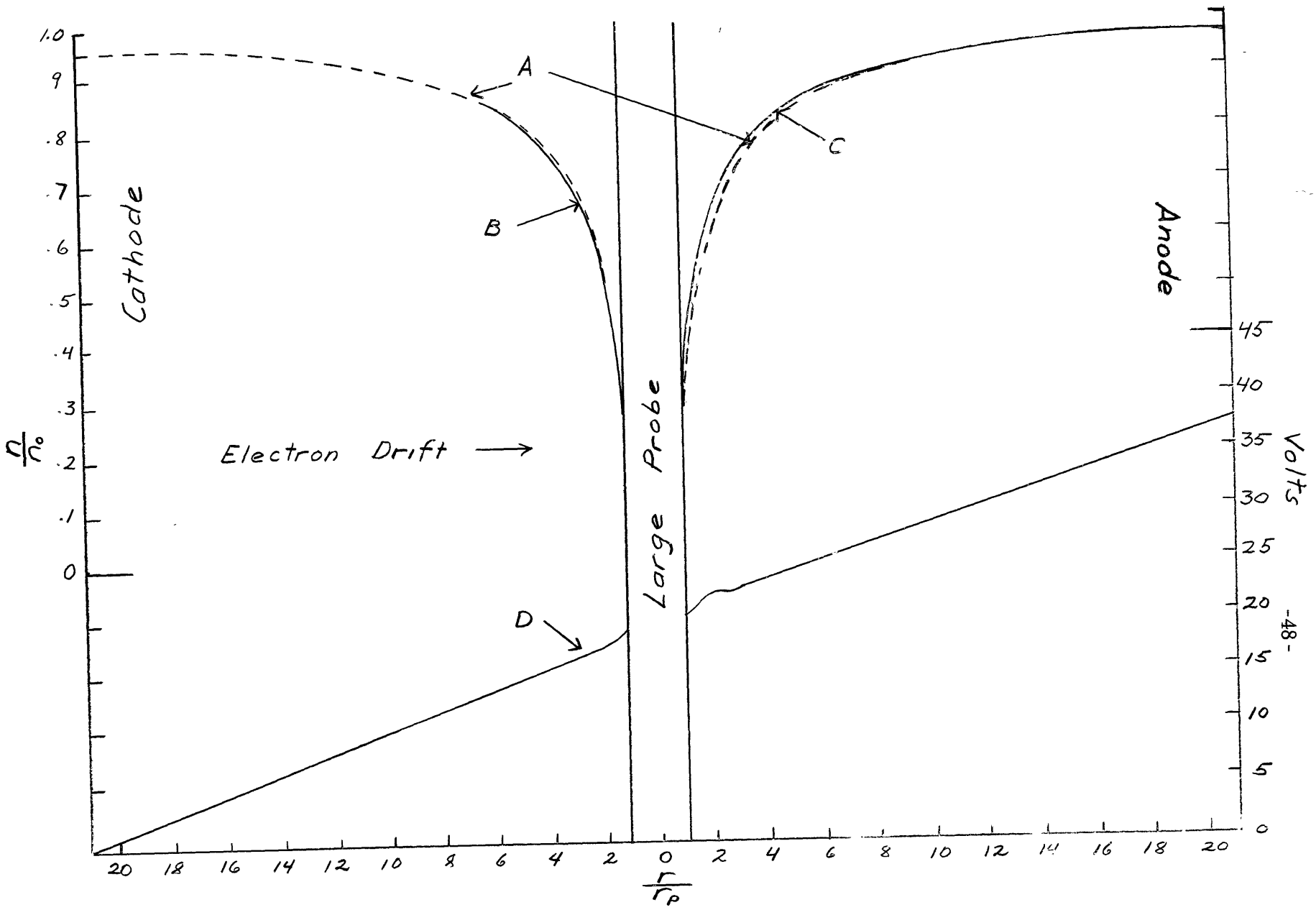

Fig 30 Composite: Large Probe Near Plasma Potential

These perturbations also appear to be of the right order of magnitude.

Anode-side determinations do not agree as well. Although the perturbation becomes less negative as large probe voltage increases, it is never positive.

Fig. 29 and 30 illustrate the comparison between the experimentally determined perturbation and the theoretically predicted perturbation. Fig. 29 corresponds to data taken when the large probe is at floating potential, while Fig. 30 is for the large-probe at its most positive potential. Curves A represent the density perturbation determined from the calculated Q's, these are symmetrical about the large-probe; curves B are the density perturbations determined from small-probe data; and curves C are the small-probe measurements of plasma potential. All curves are plotted as a function of r/r_p. The density curves emphasize the agreement between experiment and theory, even for anode-side data.

F. Plasma Density from Large-probe Data

Another check of the validity of Waymouth's theory can be made using Eq. III-7 which is

$$n_p = n_o / 1+Q_T$$

or

$$n_o = n_p(1 + Q_T)$$

n_p is the plasma density at the sheath boundary as determined from the uncorrected large-probe curve plasma potential knee. n_o is the density in the undisturbed plasma. This equation can be put in terms of the electron saturation current as

$$I_o = I_p (1 + Q_T)$$

or

$$I_o = I_p (1 + Q_e)$$

since $Q_i \approx 0$ at positive probe potentials. I_p is the experimentally determined large-probe electron saturation current and I_o is the saturation current that would be expected on the basis of the unperturbed plasma density. I_p can be determined from the large-probe curves (Figs 23 and 24) as 0.084 amps, cathode-side and 0.090 amps, anode-side. The Tables to follow summarize results of Waymouth's correction using (1) the experimentally determined Q_e's; (2) the calculated Q_e based on the ion temperature of 6700°K as determined from the large-probe curve best fit (Figs. 9 and 10); and (3) Q_e calculated on the basis of an ion temperature of 500°K which might have been estimated.

The results of these calculations are compared to the experimental I_o determined from the small-probe current at plasma potential, when at its furthest position from the large-probe, and the relative areas of the probes. For cathode-side data

$$I_o/i_o = \frac{\text{A (large-probe)}}{\text{A (small-probe)}}$$

or

$$I_o = (4.2 \times 10^{-4} \text{ amps})\ (3.7 \times 10^{-4}/3.5 \times 10^{-7})$$

and

I_o(cathode-side) = 0.444 amps. Similarly for anode-side data, $I_o = (4.4 \times 10^{-4}$ amps)(3.7/3.5) or I_o (anode-side) = 0.465 amps. The summarizing tables are:

I Large-probe Electron Saturation Current Correction: Cathode-side

Method of Determination	Q_e	I_o(amps)	Correction Factor
Experimental (ratio of areas)	---	0.444	1.00
Correction using:			
Calculated Q_e (V_i=6700°)	4.2	0.436	1.02
Calculated Q_e (V_i=500°)	6.3	0.613	0.73
Experimental Q_e	5.0	0.504	0.88
Uncorrected (large-probe curve saturation current)	---	0.084	5.30

II Large-probe Electron Saturation Current Correction: Anode-side

Method of Determination	Q_e	I_o(amps)	Correction Factor
Experimental (ratio of areas)	---	0.465	1.00
Correction using:			
Calculated Q_e(V_i=6700°)	4.2	0.468	0.99
Calculated Q_e(V_i=500°)	6.3	0.656	0.71
Experimental Q_e	3.3	0.386	1.21
Uncorrected (large-probe curve saturation current)	---	0.090	5.20

Even though neither the slight difference ($\sim 10\%$) between electron temperature as determined from large-probe data and that from small-probe data nor the changing effective area of the large probe was taken into consideration, this table should be equivalent to a plasma density comparison within experimental error. Note the extremely good agreement between the corrected I_o based on the calculated Q_e ($V_i = 6700°$) and I_o determined from the ratio of areas calculation.

G. High Ion Temperature

An ion temperature of about 6700°K was determined by the best calculated large-probe fit of the experimental data. This is, of course, extremely high. A first approximation of ion temperature can be made, neglecting charge transfer, by equating power input to the ion component of the discharge to ion energy loss due to elastic collisions.

$$e\mu_i E^2 = u\nu_c f$$

where u is the average energy of the ions and

$$f = 8/3 \frac{mM}{(m + M)^2} \quad (1 - V_g/V_i)$$

is the average energy loss per collision by particles M expressed as a fraction of the average energy of these particles[17]. Considering both Hg_+ - He and Hg_+ - Hg collisions, $V_i = 0.12$ ($\sim$1400°K). The fraction of energy loss in an Hg_+ - Hg hard sphere collision is 2/3 while in a charge exchange collision it is $\approx$1. Therefore, even though the Hg pressure is very much less than the He pressure, Hg_+ - Hg collisions dominate the result. If Hg_+ - Hg collisions are ignored, the calculated ion temperature is approximately equal to that determined by the curve fit.

An examination of Fig. 8 also indicates a high ion temperature, since for lower ion temperatures total Q_T is greater and the density perturbation resulting from this Q_T is much greater than was observed.

Although not very reliable, large-probe ion saturation currents were very large indicating high V_i. The results of Tonks[18], who concluded that

the ions arrive at the sheath boundary with an energy approximately equal to the electron mean kinetic energy, for the case of long mean free paths and no collisions, does not apply here In this case, the distance that the ambipolar electric field extends, and over which the ions are accelerated to the probe is several probe radii; that is, large in comparison to the ion mean free path. The ions therefore make many collisions on their way to the probe.

Difficulties may also arise from a possible non-Maxwellian ion velocity distribution, but this is unlikely since

$$v_e = 5 \times 10^5 \text{ m/sec}$$

while

$$v(\text{drift}) = 150 \text{ m/sec}$$

Another consideration is the increasing sheath thickness on the large-probe as its potential is made positive. The increased effective area (~15% maximum for the voltages considered) results in an increase in electron saturation current which has the same effect on the region of the large-probe curve just beyond plasma potential as does a large Q_i, which is, as the potential of the large-probe is made positive with respect to plasma potential, the repelling of ion current is reflected as an increase in electron current. Thus, the fitting could result in a larger V_i than really exists.

VI Inherent Complications

Waymouth treated the perturbation problem as one dimensional in spherical coordinates including no drift current effects or axial electric fields which necessarily exist in the discharge tube used in this experiment because of its cylindrical geometry. Thus, to emphasize, the presence of the discharge current and the axial electric field required to maintain it, introduce complications not present in the theory.

As a consequence of these complications, the tube exhibited the phenomena of wakes on the electron downstream side of both large-probe and spider. The response of a 1P21 photo multiplier tube without filters is plotted in Fig. 31 and Fig. 32 with the discharge reversed, as a function of distance along the tube axis. The solid lines are for the large-probe at floating potential, while the dotted lines are for the large-probe drawing maximum current. These curves show that increased brightness immediately on the electron downstream side of both large probe and spider is followed by a dark space. The effect is repeated until the disturbance is damped out.

B. T. Barnes[19] has studied similar phenomena. The large-probe wake can be explained by a superposition of the large-probe's perturbing electric field upon the electric field which supports the discharge. When the probe is at potentials less than plasma potential, the resultant electric field on the anode-side of the large-probe is greater than the discharge supporting electric field. This accelerates electrons which causes increased ion production and results in a brighter region. A dark space occurs just beyond the bright region most probably due to continuity of current requirements in the discharge.

On the cathode-side of the large-probe intensity dips since the resulting electric field is less than the discharge supporting electric field. Here, electron

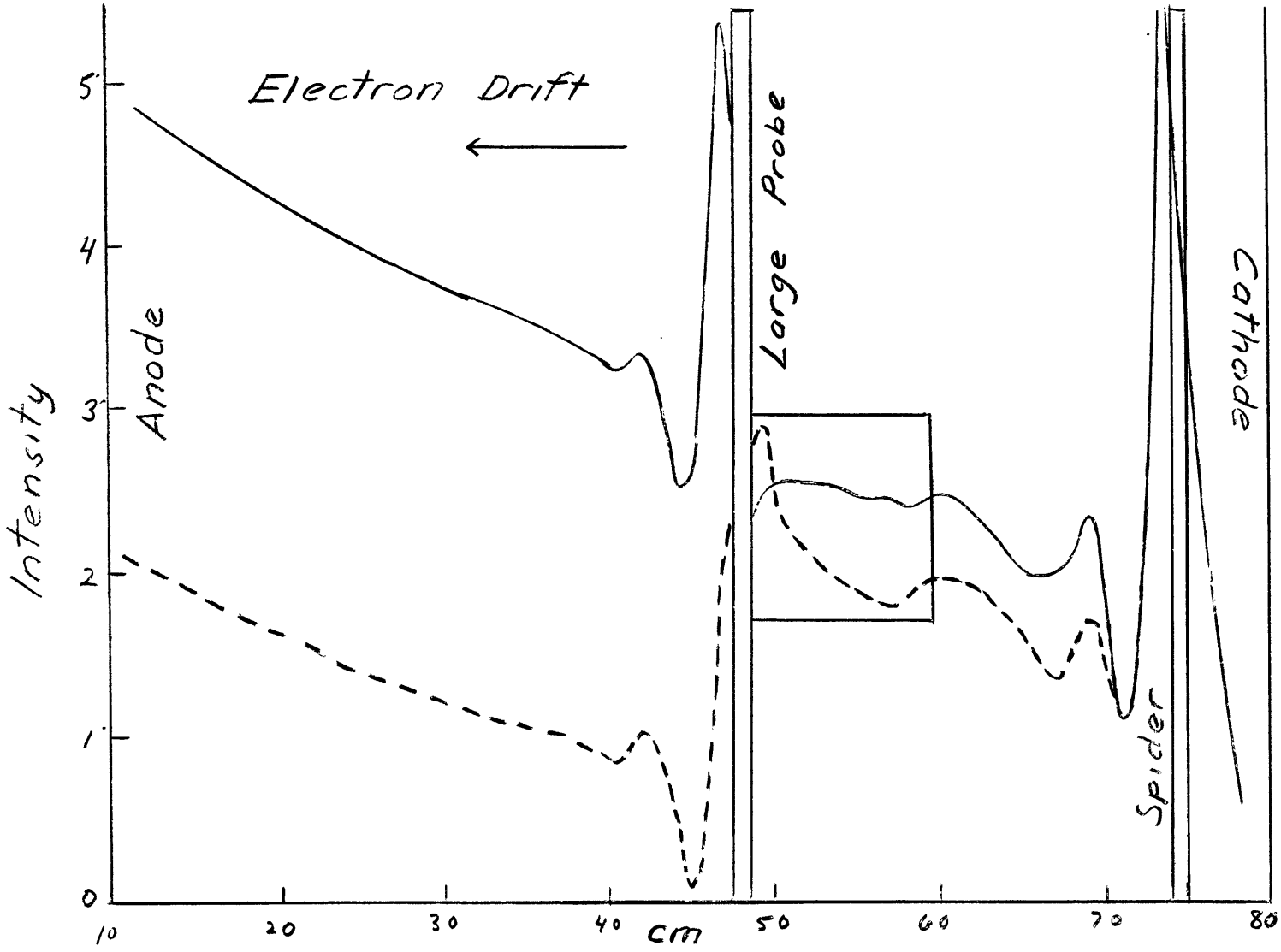

Fig. 31. Intensity Measurements: Cathode-Side Data

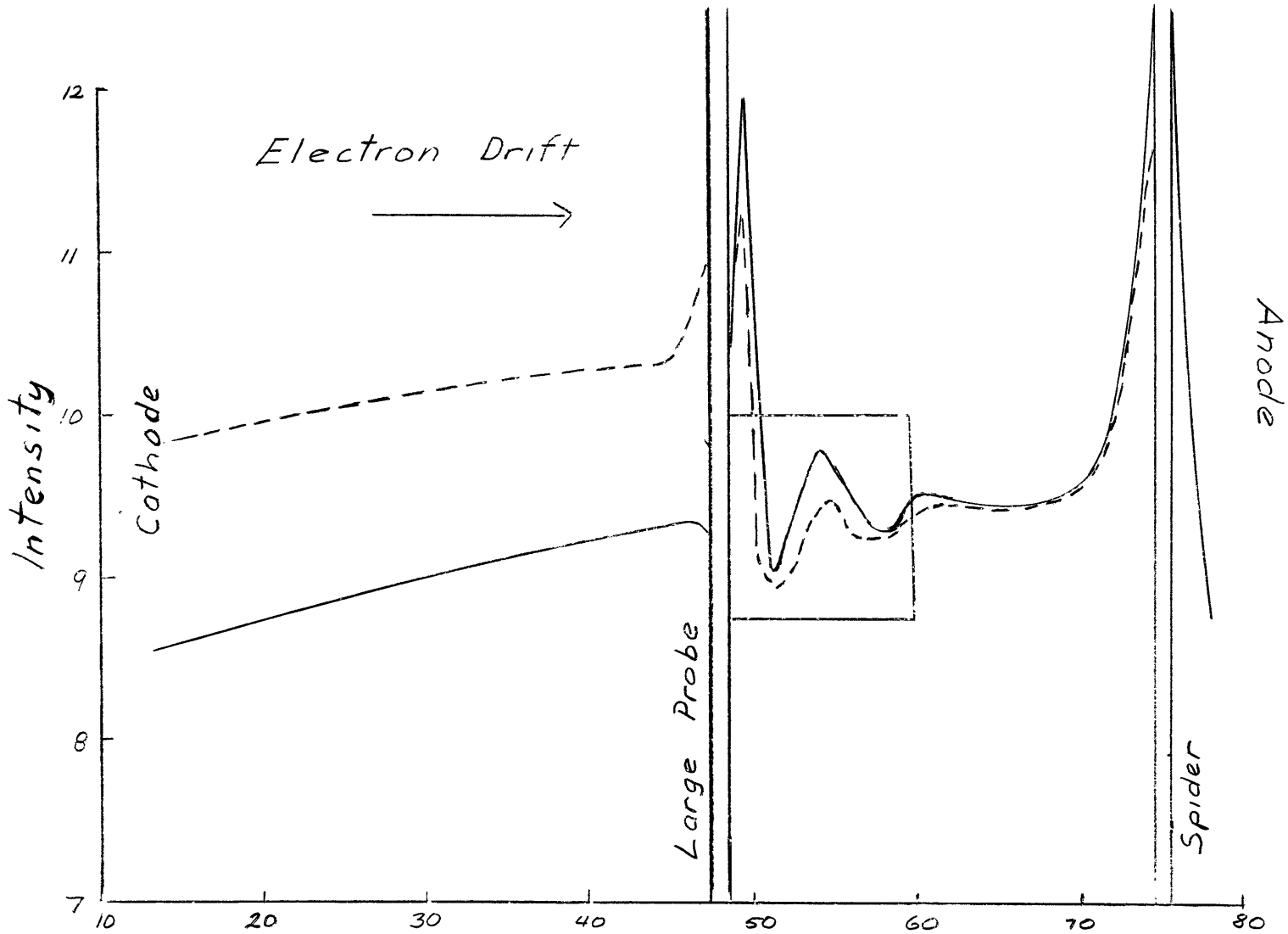

Fig. 32. Intensity Measurement: Anode - Side

energy and particle density can be expected to be lower than in the non-wake regions of the plasma.

The wake present at the spider can be explained analogously, since this glass support is at floating potential which is several volts negative with respect to plasma potential.

Figs. 33 and 34 are enlargements of the outlined areas of Figs. 31 and 32 respectively. They represent the regions of the discharge within which small probe curves were taken and show the variation of electron temperature with light intensity, while the large probe is at floating potential. Electron temperature increases at the brighter regions of the discharge as is expected.

For cathode-side data, when the large-probe is somewhat above plasma potential, the dotted lines indicate increased brightness close to the probe. This also is to be expected because the plasma is now perturbed positively.

Therefore, for the large-probe at floating potential, the wake effects cause a depletion in density in addition to the theoretical density perturbation, for cathode-side data. This density depletion decreases with increasing large-probe voltages as is indicated by the intensity curve reversal. This effect may account for the larger discrepancies between the experimental and calculated Q_T's when the large-probe is at floating potential, than the Q_T discrepancies for higher large-probe voltages. It also may be the reason for the consistent deviation of the last point from the straight line in Figs. 11-16. Although not checked extensively, at very negative large probe voltages the plasma density at this small-probe position was the only one which varied from the floating potential determination.

Fig. 32 indicates that although there is some decrease with increasing probe potential, wake effects on the anode-side of the large-probe have a

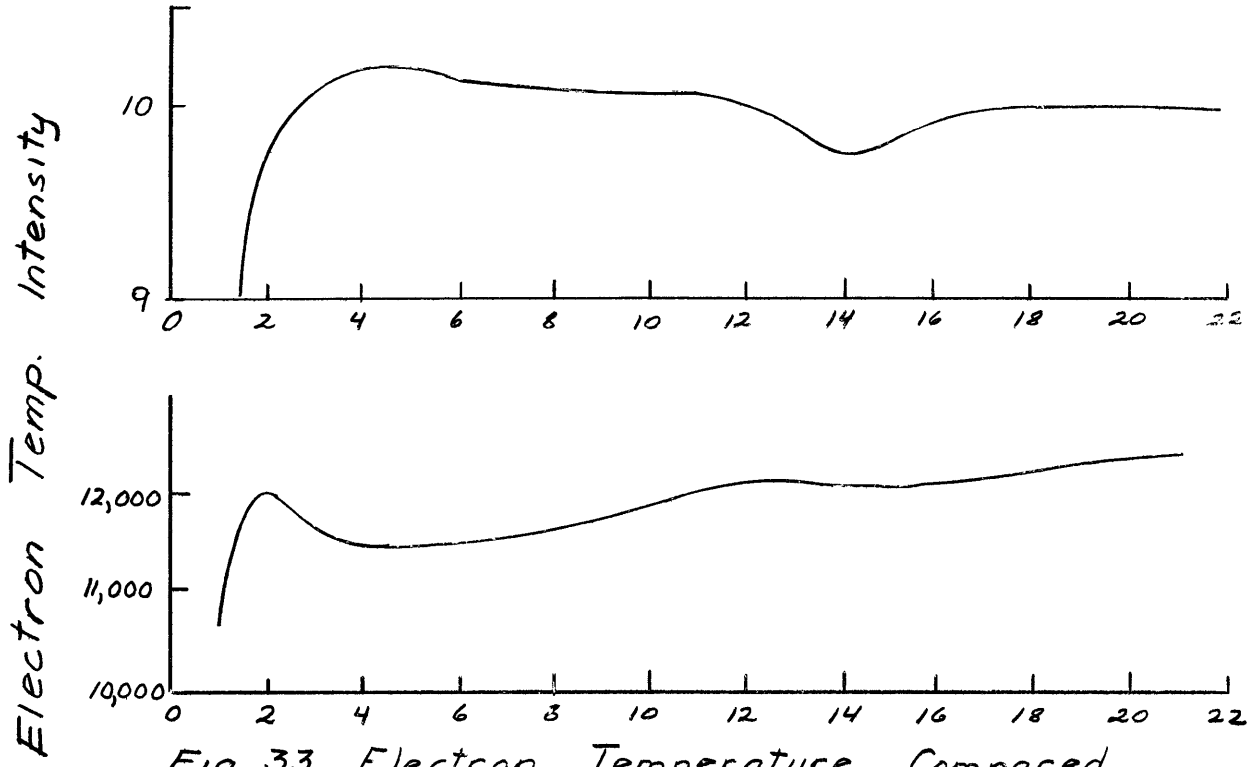

Fig. 33. Electron Temperature Compared to Intensity : Cathode Side

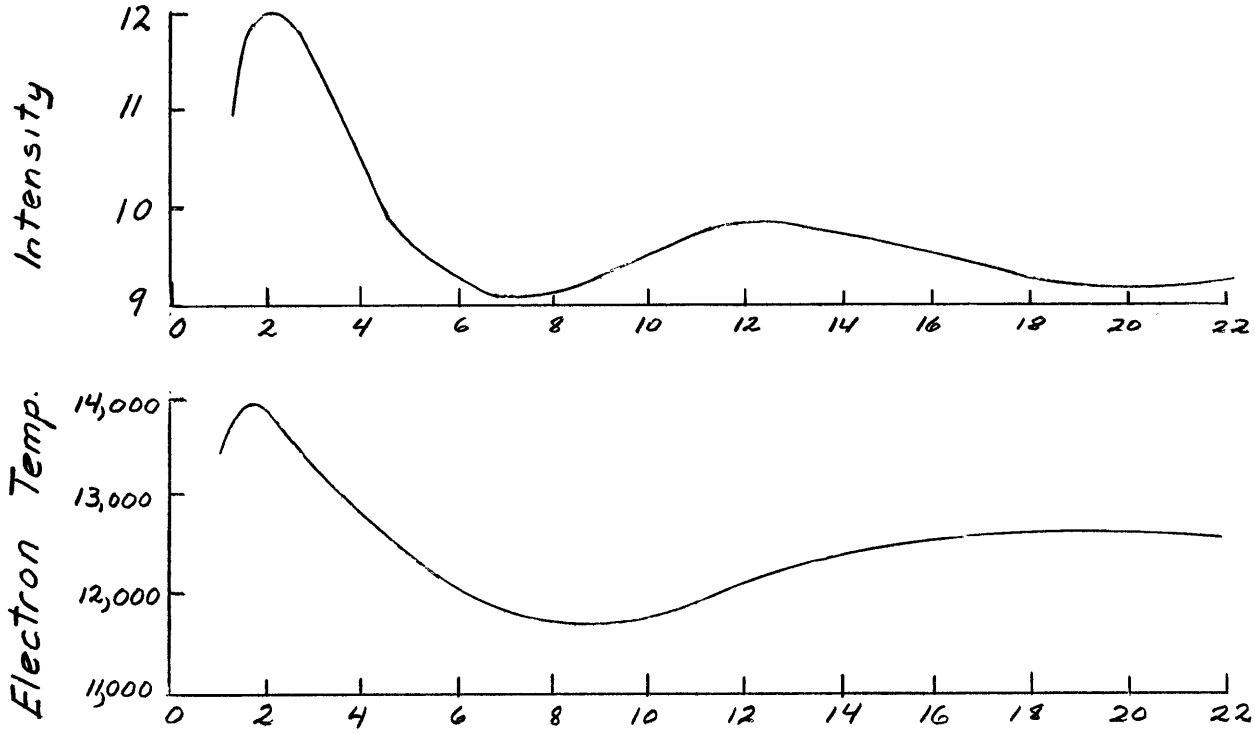

Fig. 34. Electron Temperature Compared to Intensity : Anode Side

great influence at all potentials. This may be due to discharge current adjustments for this data which maintain electron downstream currents at 0.6 amps necessitating larger upstream currents ($\sim$ 0.7 amps maximum). These strong wake effects may also account for the lack of agreement between the small probe density data (fig. 17-22) and the theory since this data did not show the theoretical 1/r dependence.

Figs. 35 and 36 further illustrate the effects of wakes on the experiment. Plasma potential minus floating potential, as determined from the small-probe curve photographs, is plotted for the various large-probe potentials as a function of r/r_p. These plots also indicate changing electron (and ion) temperature which is a direct violation of Waymouth's assumption that electron temperature be constant.

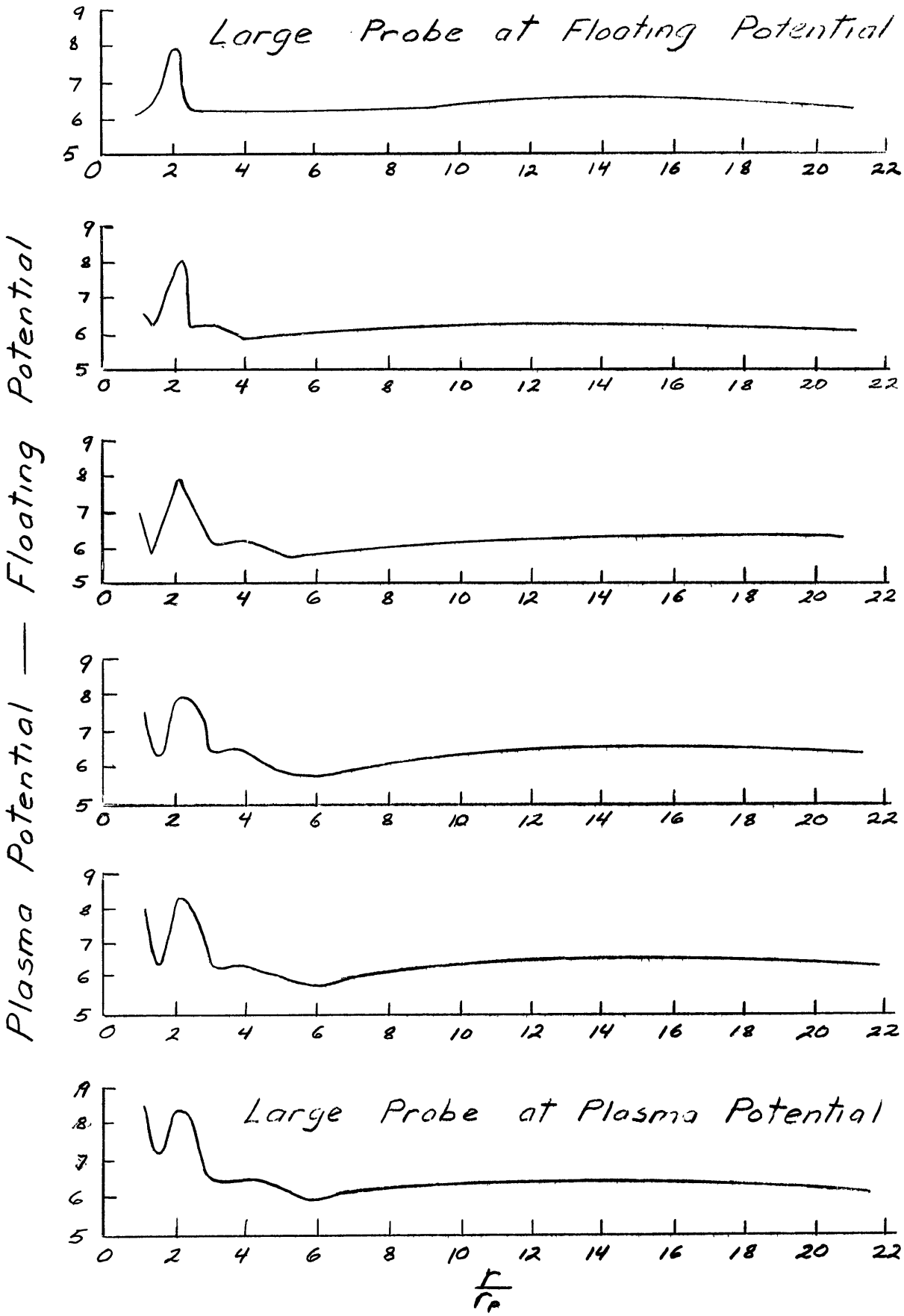

Fig. 35. Plasma Pot - Floating Pot: Cathode Data

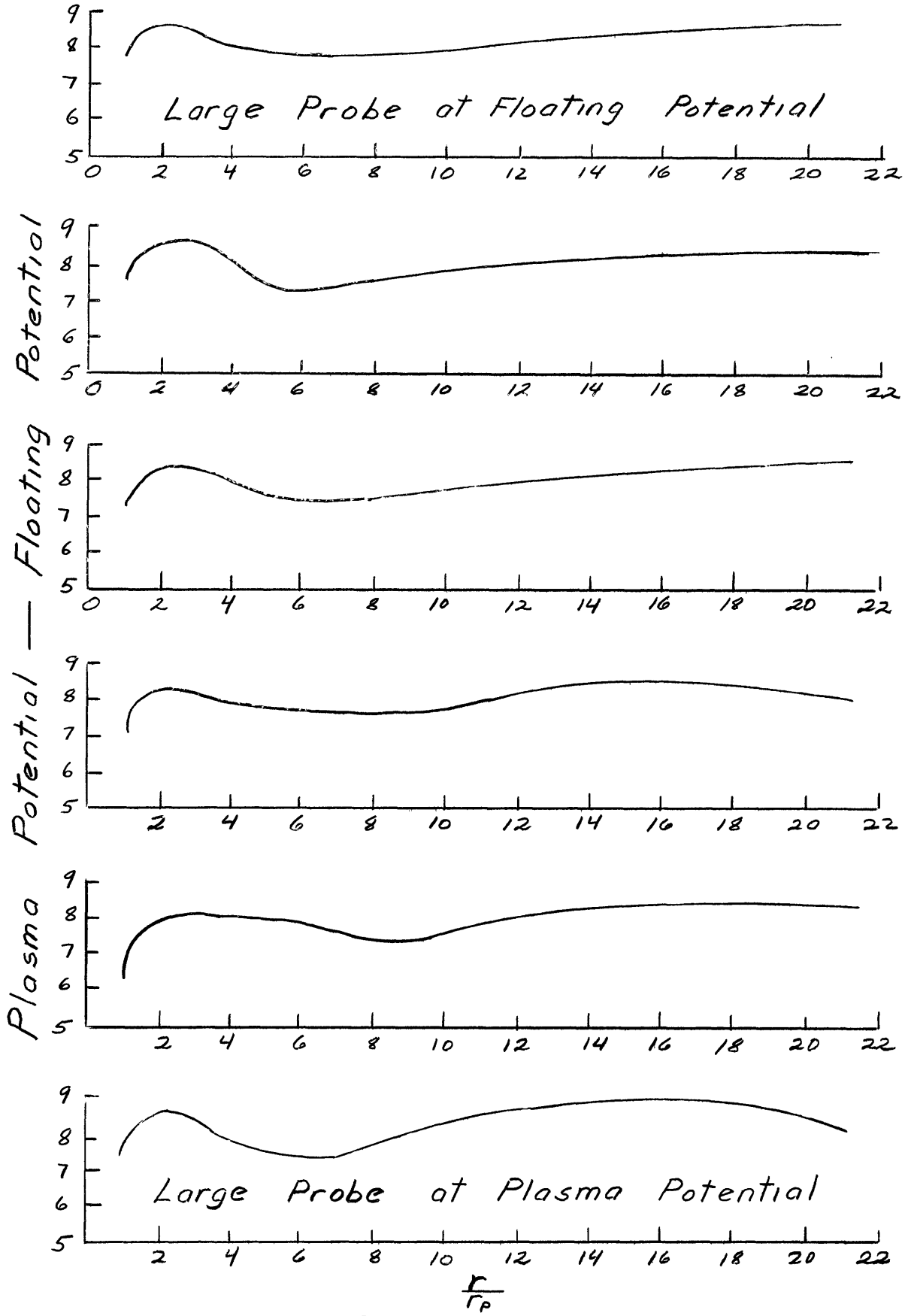

Fig. 36. Plasma Pot. — Floating Pot: Anode Data

VII Conclusion

The purpose of this experiment was to examine the validity of J. Waymouth's theory for Langmuir probe analysis when Langmuir's requirement that probe dimensions be smaller than the mean free paths of all plasma particles is not valid. This violation results in density gradients being set up in the plasma which cause ions and electrons to diffuse to the sheath region and the probe's electric field to penetrate the plasma.

Waymouth (Section III) treats the perturbation as a problem in ambipolar diffusion subject to the assumptions that the mean free paths of all plasma particles are comparable to or smaller than probe dimensions and much greater than the thickness of the probe sheath. The results are expressed in terms of a parameter Q_T which is approximately equal, at zero sheath potential, to the sum of the ratios of probe size to electron mean free path and probe size to ion mean free path. Predictions of the theory consist of:

1) A $1/r$ density dependence, the magnitude of which depends upon Q_T which in turn depends upon sheath voltage (Eq. III-5).
2) A perturbation of the plasma potential, which is, for calculations based upon the discharge tube used in this experiment, negative for probe potentials near floating potential and positive for probe potentials near plasma potential (Fig. 26).

The experiment consisted of examining the plasma perturbation caused by a large probe which violates Langmuir's conditions, with a small probe for which Langmuir's conditions are valid. By reversing the discharge, small probe data could be taken on both the anode- and the cathode-sides of the large probe. Results for cathode-side data consist of:

1) A definite 1/r density dependence (Fig. 11-16). The correct functional dependence of the density perturbation upon the large-probe sheath voltage is also well established (Fig. 25).
2) The perturbation of the plasma potential agrees well with theory, being negative for large-probe voltages near floating potential and positive for large-probe voltages near plasma potential. These perturbations also appear to be of the correct order of magnitude (Fig. 27).

Anode-side results do not agree as well. They are:

1) The density perturbation does not have a 1/r dependence (Fig. 17-22). Although the density perturbation increases with increasing voltage, it does not have the correct large-probe sheath voltage dependence (Fig. 28).
2) Although the potential perturbation becomes less negative with increasing large probe voltage, it remains negative for all potential values.

In most instances, disagreement between theory and experiment could be accounted for by the wake phenomena present in the discharge (Figs. 31 and 32). These wakes were caused by drift effects necessarily present in a discharge tube of cylindrical geometry. Waymouth's theory as the solution of a one-dimensional problem in spherical coordinates, does not take into account the wake phenomena. The validity of the extension of Waymouth's theory to Langmuir probes in magnetic fields (Ref. 6 part II of the R. L. E. report) is doubtful since these wake effects would be much more pronounced and would probably dominate any experimental data.

In Section VI-F, electron density, as determined from small-probe data, was compared to that found by applying Waymouth's correction to the apparent density, as determined from the experimental large-probe curve

knee. The comparison showed a remarkable agreement (Tables I and II).

In order to calculate the Q parameters, the ion temperature was needed. This temperature, as determined from the calculated large-probe curve fit (Figs. 9 and 10), was higher than plausible. Yet, it may indicate that ion temperature is greater than is usually assumed in similar discharges.

In concluding, it may be said that this experiment has established the validity of J. Waymouth's theory for the perturbation of a plasma by a probe. Although discrepancies did arise, they are most probably due to wake effects present in the discharge. Waymouth's theory can be expected to give an accurate prediction of a plasma disturbance by a probe especially under normal conditions when the ratios of probe size to mean free paths are more reasonable. When Langmuir's condition is violated, Waymouth's theory can be used to predict true plasma density within the error of experiment.

Although the discharge tube was constructed with an additional gas inlet tube, time did not permit further experimentation with different rare gases at different pressures. These experiments would have given further insight into the perturbation problem and the predictions of Waymouth's theory.

For all the difficulties presented by the wakes, they themselves could be the basis of further investigation. They appear to be essentially the same phenomena as moving striations often found in low pressure discharges, but could be studied more easily since they are sationary. Plots of plasma potential minus floating potential, like those of Figs. 35 and 36 could give considerable insight into ion behavior in these wakes, since both electron temperature and density can be determined.

Appendix I Tube Processing

The discharge tube, with an attached mercury vial in a dewar of cold water, was sealed on the manifold of an oil diffusion pump. Before the diffusion pump was operated, a rotary forepump brought the pressure down to microns. High pressures were measured with a Pirani gauge while low pressures were determined with an ionization gauge.

At a pressure of 5×10^{-5} mm Hg the tube was baked at 400° C for a length of time necessary to bring the pressure down to 5×10^{-6} mm Hg. The cold trap was also baked with a separate heater. The cathodes were then activated simultaneously by drawing current through them raised in small steps to 3 amperes.

When the pressure had again reached 5×10^{-6} mm Hg, the ovens were shut off and the tube was allowed to cool to room temperature. At this time a liquid nitrogen dewar was used with the cold trap.

The anodes were then out gassed with a radio frequency induction heater The tube was rebaked with the cold trap in place, and the filaments were reactivated. When the pressure reached 5×10^{-6} mm Hg , the tube was again allowed to cool to room temperature.

At room temperature, the tube was filled with helium to a pressure of 1 mm Hg, lit, turned off, and pumped down again until the discharge appeared to be clean. Then the tube was disconnected from the vacuum system.

The liquid mercury envelope seal was broken and mercury was driven into the tube. The mercury vial was then taken off. The processing was completed by flashing the barium getter.

Appendix II

Calculation of Sheath Thickness

An approximation to the large-probe sheath thickness can be made using the Child-Langmuir parallel-plate space-charge equation.

$$J = \frac{4\epsilon_o}{9} \sqrt{2e/m} \frac{V_s^{-3/2}}{d^2}$$

where J is large-probe current density, V_S is sheath voltage, and d is sheath thickness.

For $V_S = -8.0$ volts and ion saturation current = 1.0 ma,

$J_i = 3.0$ amps/m^2

and

d = 0.17 mm

Similarly, for $V_S = +8.0$ volts and electron saturation current = 0.1 amps,

$J_e = 3.0 \times 10^2$ amps/m^2

and

d = 0.4 mm

Appendix III Constructed Large-probe Curve

$V_e = 0\ 87$ ev $\qquad V_i = 2/3\ V_e$

$\frac{V_s}{V_e}$	$\frac{\Delta V}{V_e}$	$\frac{V_p}{V_e} = \frac{V_s}{V_e} + \frac{\Delta V}{V_e}$	"i" $= \frac{1}{1+Q_T}\epsilon_e$
-5.0	-0.626	-5.626	0.0045
-4.0	-0.595	-4.595	0.0118
-3.0	-0.520	-3.520	0.0248
-2.0	-0.344	-2.344	0.0552
-1.5	-0.172	-1.672	0.0797
-1.0	+0.0487	-0.951	0.109
-0.4	0.378	-0.022	0.146
-0.2	0.511	+0.311	0.158
0	0.640	0.640	0.169
0.04	0.672	0.712	0.171
0.08	0.687	0.767	0.172
0.20	0.748	0.948	0.176
0.40	0.806	1.206	0.180
0.60	0.892	1.492	0.185
1.00	0.906	1.960	0.191

References

1. I. Langmuir and H. M. Mott-Smith, Gen. Elec. Rev. 27, 499; 538; 616; 762; 810 (1924)

2. B. Davydov and L. Zmanovskaja, Tech. Phys. (U.S.S.R.) 3, 715 (1936)

3. R. L. F. Boyd, Proc. Phys. Soc. (London) 64B, 795 (1951)

4. I. M. Cohen, The Physics of Fluids 6, 1492 (1963)

5. G. Ecker, K. S. Masterson and J. J. McClure, UCRL - 10128, March (1962)

6. J. F. Waymouth, R. L. E. Tech. Rpt. 406, M.I.T., December (1962) [To be published in the Physics of Fluids, November (1964)]

7. C. H. Su and S. H. Lam, The Physics of Fluids 6, 1479 (1963)

8. H. M. Mott-Smith and I. Langmuir, Phys. Rev. 34, 876 (1929)

9. W. Verweij, Probe Measurements and Determination of Electron Mobility in the Positive Column of Low-Pressure Mercury-Argon Discharges, Ph.D. Thesis, University of Utrecht (1960) (also Physica 25, 980 (1959))

10. T. Fohl, Particle and Energy Fluxes in Weakly Ionized Gases, Ph.D. Thesis, M.I.T., (1963)

11. R. M. Howe, J Appl. Phys. 24, 881 (1953)

12. J. F. Waymouth, Pulse Technique for Probe Measurements in Gas Discharges, J. Appl. Phys. 30, 1404 (1959)

13. J. F. Waymouth and F. Bitter, J. Appl. Phys. 27, 122 (1956)

14. L. M. Chanin and M. A. Biondi, Phys. Rev. 107, 1219

15 F. R. Kovar, Phys. Rev. 133, A681, 1964

16. T. Okuda and K. Yamamoto, J. Phys. Soc. Japan 11, 177 (1956)

17. A M. Cravath, Phys. Rev. 36, 248 (1930)

18. L. Tonks and I. Langmuir, Phys. Rev. 34, 876 (1929)

19. B. T. Barnes, J. Appl. Phys. 33, 11, 3319 (1962)